



1 **The control of hydrogen sulfide on benthic iron and**  
2 **cadmium fluxes in the oxygen minimum zone off Peru**

3

4 Anna Plass<sup>1\*</sup>, Christian Schlosser<sup>1</sup>, Stefan Sommer<sup>1</sup>, Andrew W. Dale<sup>1</sup>, Eric P.  
5 Achterberg<sup>1</sup>, Florian Scholz<sup>1\*</sup>

6 <sup>1</sup>GEOMAR Helmholtz Centre for Ocean Research Kiel, Wischhofstraße 1-3, 24148  
7 Kiel, Germany

8 \*Correspondence to: Anna Plass ([aplass@geomar.de](mailto:aplass@geomar.de)), Florian Scholz  
9 ([fscholz@geomar.de](mailto:fscholz@geomar.de))

10



11 **Abstract**

12 Sediments in oxygen-depleted marine environments can be an important sink or  
13 source of bio-essential trace metals in the ocean. However, the key mechanisms  
14 controlling the release from or burial of trace metals in sediments are not exactly  
15 understood. Here, we investigate the benthic biogeochemical cycling of Fe and Cd in  
16 the oxygen minimum zone off Peru. We combine bottom water profiles, pore water  
17 profiles, as well as benthic fluxes determined from pore water profiles and in-situ from  
18 benthic chamber incubations along a depth transect at 12° S. In agreement with  
19 previous studies, both concentration-depth profiles and in-situ benthic fluxes indicate  
20 a Fe release from sediments into bottom waters. Diffusive Fe fluxes and Fe fluxes from  
21 benthic chamber incubations are roughly consistent ( $0.3 - 17.1 \text{ mmol m}^{-2} \text{ y}^{-1}$ ),  
22 indicating that diffusion is the main transport mechanism of dissolved Fe across the  
23 sediment-water interface. The occurrence of mats of sulfur oxidizing bacteria on the  
24 seafloor represents an important control on the spatial distribution of Fe fluxes by  
25 regulating hydrogen sulfide ( $\text{H}_2\text{S}$ ) concentrations and, potentially, Fe sulfide  
26 precipitation within the surface sediment. Removal of dissolved Fe after its release to  
27 anoxic bottom waters is rapid in the first 4 m away from the seafloor (half-life < 3 min)  
28 which hints to oxidative removal by nitrite or interaction with particles in the benthic  
29 boundary layer. Benthic flux estimates of Cd are indicative of a flux into the sediment  
30 within the oxygen minimum zone. Fluxes from benthic chamber incubations (up to  $22.6$   
31  $\mu\text{mol m}^{-2} \text{ y}^{-1}$ ) exceed the diffusive fluxes ( $< 1 \mu\text{mol m}^{-2} \text{ y}^{-1}$ ) by a factor  $> 25$ , indicating  
32 that downward diffusion of Cd across the sediment-water interface is of subordinate  
33 importance for Cd removal from benthic chambers. As Cd removal in benthic chambers  
34 co-varies with  $\text{H}_2\text{S}$  concentrations in the pore water of surface sediments, we argue  
35 that Cd removal is mediated by precipitation of CdS within the chamber. A mass  
36 balance approach, taking into account the contributions of diffusive fluxes and fluxes  
37 measured in benthic chambers as well as Cd delivery with organic material suggests  
38 that CdS precipitation in the near-bottom water could make an important contribution  
39 to the overall Cd mass accumulation in the sediment solid phase. According to our  
40 results, the solubility of trace metal sulfide minerals ( $\text{Cd} \ll \text{Fe}$ ) is a key-factor  
41 controlling trace metal removal and consequently the magnitude as well as the  
42 temporal and spatial heterogeneity of sedimentary fluxes. We argue that depending on  
43 their sulfide solubility, sedimentary source or sink fluxes of trace metals will change  
44 differentially as a result of declining oxygen concentrations and an associated



45 expansion of sulfidic surface sediments. Such a trend could cause a change in the  
46 trace metal stoichiometry of upwelling water masses with potential consequences for  
47 marine ecosystems in the surface ocean.

48

49

## 50 **1. Introduction**

51

### 52 **1.1 Scientific rationale**

53 The world's oceans are losing oxygen (e.g. Keeling et al. 2010; Stramma et al.  
54 2010; Helm et al. 2011). In total around 2 % of oxygen has been lost over the past five  
55 decades (Schmidtko et al., 2017) and an expansion of oxygen minimum zones (OMZs)  
56 in the tropical oceans has been documented over the same timespan (Stramma et al.,  
57 2008). The biogeochemical cycling of several nutrient type trace metals (TMs) is likely  
58 to be particularly susceptible to changing oxygen concentrations as they occur in  
59 different oxidation states (e.g. Fe, Mn, Co) and/or are precipitated as sulfide mineral in  
60 anoxic-sulfidic environments (e.g. Zn, Cd). However, with the exception of Fe (Dale et  
61 al., 2015a; Lohan and Bruland, 2008; Rapp et al., 2018; Schlosser et al., 2018; Scholz  
62 et al., 2014a), little information is available on how other TM fluxes will respond to  
63 ocean deoxygenation. As certain TMs are essential for the growth of marine organisms  
64 (e.g. Fe, Mn, Co, Ni, Zn, Cd), TM availability can (co-)limit primary productivity and  
65 therefore affect oceanic carbon sequestration through the biological pump (Saito et al.,  
66 2008; Moore et al., 2013; Morel et al., 2014). As a consequence, a better  
67 understanding of how TMs respond to low oxygen conditions is essential for predicting  
68 how marine ecosystems and the carbon cycle will evolve in the future ocean, with  
69 modelling scenarios predicting a continuation of ocean deoxygenation (Bopp et al.,  
70 2002; Oschlies et al., 2008; Keeling et al., 2010)

71 Marine sediments are an important source or sink of TMs to the ocean under  
72 low oxygen conditions (Böning et al., 2004; Brumsack, 2006; Scor Working Group,  
73 2007; Severmann et al., 2010; Noble et al., 2012; Biller and Bruland, 2013; Conway  
74 and John, 2015b; Klar et al., 2018). In the OMZ off the coast of Peru, substantial fluxes  
75 of reduced Fe and other TMs across the sediment-bottom water interface have been



76 documented (Noffke et al., 2012; Scholz et al., 2016) or inferred (Hawco et al., 2016).  
77 While a number of studies have addressed biogeochemical processes that lead to  
78 benthic Fe release, the key biogeochemical processes and conditions that control the  
79 sedimentary release or burial of other TMs are still poorly constrained. Moreover, a  
80 detailed picture of removal or stabilization processes and rates that take place in the  
81 highly dynamic benthic boundary layer is lacking.

82 In this article, we compare the benthic biogeochemical cycling of Fe and Cd. It  
83 has been established that the Peruvian OMZ represents a source of dissolved Fe to  
84 the ocean (Noffke et al., 2012; Fitzsimmons et al., 2016; John et al., 2018). In contrast,  
85 earlier studies have demonstrated that OMZs represent a sink for Cd (Janssen et al.,  
86 2014; Böning et al., 2004). Because of their contrasting tendency to form sulfide  
87 minerals and different supply pathways to the sediment, Fe and Cd can provide  
88 information about how sedimentary fluxes of different TMs may respond to declining  
89 oxygen concentrations. By comparing the benthic biogeochemical cycling of Fe and  
90 Cd across spatial and temporal redox gradients, we aim to provide general constraints  
91 on how the stoichiometry of bio-essential TMs in seawater may be affected by ocean  
92 deoxygenation.

93

## 94 **1.2. Marine biogeochemistry of iron**

95 Iron is the most abundant TM in phytoplankton and part of a range of  
96 metalloenzymes that are involved in important biological functions, such as  
97 photosynthesis or nitrogen fixation (Twining and Baines, 2013). Despite Fe being  
98 highly abundant in the continental crust, its low availability limits primary productivity in  
99 up to 30 % of the surface ocean area (Moore et al., 2013). This limitation arises from  
100 the low solubility of its thermodynamically stable form in oxic waters, Fe(III).  
101 Concentrations can reach up to ~ 1 nM when Fe(III) is kept in solution through  
102 complexation with organic ligands (Rue and Bruland, 1997; Liu and Millero, 2002; Boyd  
103 and Ellwood, 2010; Raiswell and Canfield, 2012). The thermodynamically stable form  
104 of Fe under anoxic conditions, Fe(II), is more soluble and therefore anoxic waters are  
105 typically characterized by higher dissolved Fe concentrations (up to tens of nM)  
106 (Conway and John, 2014; Vedamati et al., 2014; Fitzsimmons et al., 2016; Schlosser  
107 et al., 2018).



108 Sediments within OMZs are considered an important source of dissolved Fe and  
109 some of the highest sedimentary Fe fluxes have been observed in these regions  
110 (Severmann et al., 2010; Noffke et al., 2012). Under anoxic conditions, Fe(II) can be  
111 liberated from the sediments into pore waters from Fe-(oxyhydr)oxides through  
112 reductive dissolution by microbes or abiotic reduction with H<sub>2</sub>S (Canfield, 1989). In the  
113 absence of oxygen, dissolved Fe(II) escapes the rapid re-oxidation and subsequent  
114 (oxyhydr)oxide precipitation and can, therefore, diffuse from pore waters into bottom  
115 waters. However, in anoxic OMZs, where denitrification takes place, Fe(II) can also be  
116 re-oxidized by either biologically by nitrate-reducing microbes or abiotically by nitrite  
117 (Straub et al., 1996; Carlson et al., 2013; Scholz et al., 2016; Heller et al., 2017). The  
118 solubility of Fe in sulfidic (i.e. NO<sub>3</sub><sup>-</sup> and NO<sub>2</sub><sup>-</sup> depleted) water is relatively high (Rickard  
119 et al., 2006) and it has been observed, that during sulfidic events dissolved Fe can  
120 accumulate in the water column (up to hundreds of nM) because of decreased Fe  
121 oxidation (Scholz et al., 2016) and stabilization as aqueous Fe sulfide complexes and  
122 clusters (Schlosser et al., 2018). However, Fe fluxes across the benthic boundary have  
123 been hypothesized to decrease as H<sub>2</sub>S accumulation in the surface sediment impedes  
124 Fe escape through precipitation of Fe sulfide minerals (Scholz et al., 2014b).

125

### 126 **1.3. Marine biogeochemistry of cadmium**

127 Even though its concentrations are one order of magnitude lower compared to  
128 Fe, Cd is abundant in phytoplankton (Twining and Baines, 2013). A function for Cd as  
129 a catalytic metal atom in the carbonic anhydrase protein has been found in diatoms  
130 (Lane and Morel, 2000) and it can also substitute Zn and enhance phytoplankton  
131 growth under Zn limitation in different phytoplankton species (Price and Morel, 1990;  
132 Lee and Morel, 1995; Sunda and Huntsman, 2000; Xu et al., 2008). Inside the marine  
133 sediments Cd can be released from the solid phase into the pore waters through the  
134 remineralization of organic matter (Klinkhammer et al., 1982; Collier and Edmond,  
135 1984; Gendron et al., 1986; Gerringa, 1990; Audry et al., 2006; Scholz and Neumann,  
136 2007). After its release to the pore water, Cd can either diffuse across the sediment-  
137 water interface, or under anoxic and sulfidic conditions, Cd is thought to be precipitated  
138 as CdS (Greenockite) (Westerlund et al., 1986; Gobeil et al., 1987; Rosenthal et al.,  
139 1995; Audry et al., 2006). Due to its low sulfide solubility, CdS can precipitate at much



140 lower H<sub>2</sub>S concentrations than FeS (Mackinawite), which is the precursor for pyrite  
141 (FeS<sub>2</sub>) (Morse and Luther, 1999).

142         The few studies on pore water concentration and benthic fluxes of Cd, mostly  
143 carried out in estuaries or coastal settings, generally concluded that the flux of organic  
144 material and the presence of H<sub>2</sub>S are the most important factors controlling the balance  
145 between Cd recycling versus precipitation and burial (e.g. Westerlund et al. 1986;  
146 Colbert et al. 2001; Audry et al. 2006; Scholz and Neumann 2007). Low oxygen regions  
147 in the ocean are considered an important sink for Cd (Janssen et al., 2014; Conway  
148 and John, 2015a; Xie et al., 2019) and sediments below OMZs are highly enriched in  
149 Cd (Ragueneau et al., 2000; Böning et al., 2004; Borchers et al., 2005; Muñoz et al.,  
150 2012; Little et al., 2015), however, the respective contributions of different Cd removal  
151 mechanism to Cd accumulation in the sediment have not been quantified.

152

#### 153 **1.4. Study area**

154         Seasonal upwelling of nutrient-rich waters off the Peruvian coast in austral  
155 winter leads to a high primary productivity in the euphotic zone (~ 300 mmol C m<sup>-3</sup> d<sup>-1</sup>)  
156 (Pennington et al., 2006). The combination of oxygen consumption through the  
157 respiration of this organic matter and low oxygen concentrations in water masses that  
158 supply upwelling regions, leads to the formation of one of the world's most intense  
159 OMZs, with complete oxygen consumption in the core of the OMZ between ~ 100 m –  
160 300 m water depth (Karstensen et al., 2008; Thamdrup et al., 2012). Upon oxygen  
161 depletion, NO<sub>3</sub><sup>-</sup> can serve as an electron acceptor for respiration, therefore,  
162 denitrification, dissimilatory reduction of NO<sub>3</sub><sup>-</sup> to ammonium (DNRA) and anaerobic  
163 ammonium oxidation (anammox) with NO<sub>2</sub><sup>-</sup> are important biogeochemical processes  
164 within the anoxic and nitrogenous water column (Lam et al., 2009; Lam and Kuypers,  
165 2011; Dalsgaard et al., 2012). The OMZ overlying the Peruvian shelf is a temporally  
166 and spatially dynamic system where biogeochemical conditions can range from fully  
167 oxic to anoxic and sulfidic. Occasional shelf oxygenation events occur mostly during  
168 El Niño events and are linked to the propagation of coastal trapped waves (Gutiérrez  
169 et al., 2008), but could be also observed during a coastal El Niño event (Lüdke et al.,  
170 2019). During such events oxygen can reach down the upper slope to 200 m – 300 m  
171 water depth (Levin et al., 2002). By contrast, sulfidic events can occur during periods



172 of stagnation, when not only oxygen but also  $\text{NO}_3^-$  and  $\text{NO}_2^-$  become depleted in the  
173 water column due to low water mass exchange. Once  $\text{NO}_3^-$  and  $\text{NO}_2^-$  are depleted,  
174 chemolithoautotrophic  $\text{H}_2\text{S}$  oxidation is impeded. Under such conditions,  $\text{H}_2\text{S}$   
175 produced by bacterial sulfate reduction in sediments can be released into the water  
176 column (Schunck et al., 2013), with the amount of  $\text{H}_2\text{S}$  being released on the Peruvian  
177 shelf reaching several  $\text{mmol m}^{-2} \text{d}^{-1}$  (Sommer et al., 2016)

178

179

## 180 **2. Methods**

181

### 182 **2.1 Sampling and sample handling**

183 In this study, data from three different types of samples were combined: (1) pore  
184 waters for the determination of benthic diffusive fluxes and to study TM cycling in  
185 sediments; (2) Benthic chamber incubations, to determine in-situ fluxes across the  
186 sediment-water interface; (3) Near bottom water profiles to determine the fate of TMs  
187 in the particle-rich and reactive benthic boundary layer.

188 Our sampling took place during RV Meteor cruises M136 and M137 in austral  
189 autumn between April and May 2017. We also compare our recent data set to benthic  
190 diffusive Fe(II) flux data from RV Meteor cruise M92, which took place in austral  
191 summer during January 2013. Our sampling stations cover the entire Peruvian shelf  
192 and slope across a transect at  $12^\circ\text{S}$  (Fig. 1). This transect covered water depths from  
193 75 m to 950 m and includes stations above, inside and below the permanent OMZ. Our  
194 sampling of pore waters and sample collection from benthic chamber incubations  
195 generally followed the methodology described in Noffke et al. (2012).

196 Short sediment cores of 30 cm to 40 cm length were retrieved with a multiple  
197 corer. Upon recovery, the cores were directly transferred into the ship's cool room  
198 ( $4^\circ\text{C}$ ). The supernatant bottom water was instantly sampled and filtered through  $0.2$   
199  $\mu\text{m}$  cellulose acetate filters (Sartorius) and acidified to  $\text{pH} < 1$  with subboiled distilled  
200  $\text{HNO}_3$ . The sediment cores were subsequently sampled in vertical sections in a glove  
201 bag under Ar atmosphere to prevent any contact with oxygen. The sediment samples  
202 were centrifuged to separate the pore waters from the sediment solid phase. Pore



203 waters were then filtered in another Ar-filled glove bag through 0.2  $\mu\text{m}$  cellulose acetate  
204 filters (Sartorius). An aliquot of 8 ml was acidified to  $\text{pH} < 1$  with subboiled distilled  
205  $\text{HNO}_3$  and stored in acid cleaned low-density polyethylene (LDPE) bottles for TM  
206 analysis. Another aliquot was taken for analysis of  $\text{H}_2\text{S}$  concentrations. Additional  
207 sediment subsamples were collected in pre-weight cups for water content and porosity  
208 determination as well as for Cd and organic C concentrations measurements in the  
209 solid phase.

210 Benthic landers that consist of titanium frames and contain two circular benthic  
211 chambers to conduct in-situ incubations were deployed on the seafloor (see Sommer  
212 et al. (2009) for details). After placement of the lander on the seafloor, the benthic  
213 chambers (internal diameter of 28.8 cm) were partially driven into the sediment,  
214 covering a sediment area of 651.4  $\text{cm}^2$ . The seawater volume that was enclosed in the  
215 chamber varied between 12 l and 18 l, depending on the insertion depth of the chamber  
216 into the sediment. Prior to incubation, the seawater contained in the chamber was  
217 repeatedly replaced with ambient seawater to replace solutes and flush out particles,  
218 which were mobilized during the insertion of the chamber into the sediment. Over the  
219 incubation time of around 32 hours, 8 consecutive samples were filtered in-situ through  
220 0.2  $\mu\text{m}$  cellulose acetate filters (Sartorius) via peristaltic pumps and collected in quartz  
221 glass tubes. All sampling tubes were acid cleaned prior to use to guarantee a TM clean  
222 sampling. After recovery of the lander, the quartz glass tubes were transferred to the  
223 laboratory and the obtained sample amount of 12 ml for each incubation time was  
224 stored in acid cleaned LDPE bottles and acidified to  $\text{pH} < 2$  with subboiled distilled  
225  $\text{HNO}_3$ . Other samples were collected simultaneously for analysis of nitrogen species.  
226 The incubated sediments within the benthic chamber were sampled after recovery of  
227 the lander and pore waters were extracted to analyze  $\text{H}_2\text{S}$  concentrations for  
228 comparison with pore water profiles from parallel MUCs.

229 To determine TM concentrations across the benthic boundary layer, we used  
230 the lander to collect water samples at a distance of 0.5, 1.0, 2.0, 3.0 and 4.0 m from  
231 the seafloor. Filter holders with 0.2  $\mu\text{m}$  polyether sulfone filters (Supor) were attached  
232 at the various depths and connected to sampling tubes that went through peristaltic  
233 pumps into gas sampling bags (Tedlar). The sampling at distances of 3.0 m and 4.0 m  
234 above the seafloor was realized by attaching the filter holders and tubing to an arm  
235 that was automatically unfolded upon placement of the lander at the seafloor. The



236 peristaltic pumps transferred the seawater from their sampling depth into the sampling  
237 bags over the same time period of the lander incubations of around 32 hours. This  
238 resulted in an average sample volume of 1.5 l per depth. All filters, tubing and sampling  
239 bags were acid cleaned prior to deployment to guarantee a TM clean sampling. Directly  
240 after sample retrieval an aliquot of 60 ml was stored in acid cleaned LDPE bottles and  
241 acidified to  $\text{pH} < 2$  for TM analysis. Another aliquot was taken for analysis of silicic acid  
242 ( $\text{Si}(\text{OH})_4$ ).

243

## 244 **2.2 Analytical methods**

245 Concentrations of Fe(II) in pore waters were measured on board directly after  
246 sample retrieval by photometry using the ferrozine method (Stookey, 1970). Other  
247 geochemical parameters in our different samples were also determined photometrical  
248 (U-2001 Hitachi spectrometer) using standard techniques (Grasshoff et al., 1999).  
249 Hydrogen sulfide concentrations were determined using the methylene blue method  
250 and silicic acid concentrations were determined using a heptamolybdate solution as  
251 reagent. Concentrations of nitrogen species were determined by an auto-analyzer  
252 (QuAatro, SEAL Analytical) using sulfanilamide as reagent (Hydes et al., 2010).

253 For TM analysis of bottom water samples we followed the procedure described  
254 by Rapp et al. (2017), where the TMs are pre-concentrated by a fully automated device  
255 (SeaFAST). After raising the sample pH to 6.4 with an ammonium acetate buffer (1.5  
256 M), a sample amount of 15 ml was loaded onto a chelating resin column, where the  
257 seawater matrix was rinsed off, before the TMs were collected into 1 ml elution acid (1  
258 M subboiled  $\text{HNO}_3$ ). Due to the smaller size of pore water samples and samples from  
259 benthic lander incubations, a half-automated device (Preblab) with a smaller sample  
260 loop and thus dead volume was applied for these sample types. On this device, sample  
261 loading and collection as well as the addition of buffer was done manually. For samples  
262 from benthic lander incubations, an amount of 3 ml and for pore waters 1 ml was  
263 needed for pre-concentration. The samples were diluted with de-ionised water (MilliQ,  
264 Millipore) to increase the sample volume to 5 ml for samples from benthic chamber  
265 incubations and to 3 ml for pore waters. The pre-concentrated samples were measured  
266 by ICP-MS (HR-ICP-MS; Thermo Fisher Element XR) and TM concentrations were  
267 quantified by isotope dilution (Rapp et al., 2017). Accuracies for replicate  
268 measurements of certified reference seawater for TMs are listed in Table 1.



269 Cadmium and Al concentrations in sediments for calculation of sedimentary Cd  
270 enrichments ( $Cd_{xs}$ ) were determined following total digestions of freeze dried and  
271 ground sediment. The sediment was digested in 40 % HF (suprapure), 65 % HNO<sub>3</sub>  
272 (suprapure) and 60 % HClO<sub>4</sub> (suprapure). Concentrations were measured by ICP-OES  
273 (VARIAN 720-ES). The reference standard MESS was used to check the digestion  
274 procedure, the accuracy was  $\pm 0.3$  % for Cd and  $\pm 1.3$  % for Al (MESS-3 Cd:  $0.24 \pm$   
275  $0.01 \mu\text{g g}^{-1}$ , recommended value  $0.24 \pm 0.01 \mu\text{g g}^{-1}$ , MESS-3 Al:  $8.59 \pm 0.11 \mu\text{g g}^{-1}$ ,  
276 recommended value  $8.59 \pm 0.23 \mu\text{g g}^{-1}$ ).

277 Organic carbon content in the sediments was determined, after removal of  
278 inorganic carbon with 0.25 mM HCl, using an Elemental Analyzer (Euro EA). Precision  
279 of the measurement was  $\pm 1$  %.

280

### 281 2.3 Flux calculations

282 Benthic diffusive fluxes ( $F_D$ ) were determined using Fick's first law of diffusion  
283 using concentration gradients between the uppermost pore water sample (0 – 1 cm)  
284 and the overlying bottom water ( $dC/dx$ ) (Boudreau, 1997):

$$285 \quad F_D = -\Phi D_{sed}(dC/dx) \quad (1)$$

286 The effective molecular diffusion coefficients of Fe and Cd for sediments ( $D_{sed}$ ) were  
287 calculated from the molecular diffusion coefficient in seawater ( $D_{sw}$ ) under standard  
288 conditions (Li and Gregory, 1974) by adjusting it to in-situ temperature, pressure and  
289 salinity applying the Stokes-Einstein Equation. We determined the diffusion  
290 coefficients for sediments as follows:

$$291 \quad D_{sed} = D_{sw}/\theta^2 \quad (2)$$

292 Tortuosity ( $\theta$ ) was calculated from porosity ( $\Phi$ ) as follows (Boudreau, 1997):

$$293 \quad \theta^2 = 1 - \ln(\phi^2) \quad (3)$$

294 Positive values represent a flux from the bottom water into the sediment pore water.

295 The fluxes from benthic lander incubations were calculated from the slopes of  
296 linear regressions, resulting from concentration changes over the incubation times.  
297 Fluxes were corrected for water volume enclosed in the benthic chamber, which was



298 determined for each deployment from the insertion depth of the benthic chamber into  
299 the sediment.

300

301

### 302 **3. Results**

303

#### 304 **3.1 Biogeochemical conditions in the water column**

305 Cruise M136 and M137 took place in April and May 2017, during the decline of  
306 a coastal El Niño event. A coastal El Niño is a local phenomenon that refers to reduced  
307 upwelling and increased sea surface temperatures off the coasts of Peru and Ecuador,  
308 with typically heavy rainfall on land. During this event in austral summer, coastal waters  
309 off Peru showed a strong positive sea surface temperature anomaly of up to 2 to 4 °C  
310 (Echevin et al., 2018; Garreaud, 2018). The warming is proposed to be a result of  
311 strong local alongshore wind anomalies and equatorial Kelvin waves propagating  
312 towards the Peruvian coast (Echevin et al., 2018; Peng et al., 2019). Due to the  
313 particular atmospheric and oceanographic conditions, the water column overlying the  
314 Peruvian shelf was oxygenated during our sampling campaign. Oxygen concentrations  
315 were > 20 µM in the water column down to around 100 m water depth. However oxygen  
316 concentrations in bottom waters directly above the seafloor on the shallowest station  
317 (station 1) were below the detection limit (> 1 µM) measured through optopodes  
318 attached to lander. The OMZ, with O<sub>2</sub> concentrations < 5 µM, extended from around  
319 120 to 400 m water depth. The water column within the OMZ was nitrogenous (i.e.  
320 NO<sub>3</sub><sup>-</sup> reducing) as indicated by the presence of NO<sub>2</sub><sup>-</sup> (≥ 4 µM), an intermediate product  
321 of denitrification (Zumft, 1997). Oxygen gradually increased to > 50 µM from below 400  
322 m towards 950 m water depth (Fig. 2). As we will compare some of our data to those  
323 of an earlier cruise (M92), the corresponding oxygen distribution across the Peruvian  
324 continental margin is shown for comparison (Fig. 2).

325

#### 326 **3.2 Benthic iron cycling**

327 Iron concentrations in near bottom waters decreased from near shore to off  
328 shore stations, from > 100 nM at the shallowest shelf station at 75 m water depth



329 (station 1) to 6 nM at 750 m water depth (station 9) (Fig. 3). At a number of stations  
330 within the OMZ (stations 3 and 4), vertical concentration gradients were observed.  
331 Here Fe concentrations decreased by 15 - 20 nM from 0.5 to 4 m above the seafloor.  
332 Multiple sampling at the shallowest shelf station (station 1) revealed that Fe  
333 concentrations were temporally variable and ranged from ~ 100 nM at the end of April  
334 to < 60 nM at the end of May 2017.

335 Concentrations of Fe(II) in pore waters were highest (up to a few  $\mu\text{M}$ ) in the  
336 upper 5 – 10 cm of the sediment cores. Downcore, concentrations decreased to > 0.2  
337  $\mu\text{M}$  (Fig. 4). At all stations, concentrations in pore waters at the sediment surface were  
338 higher than in the overlying bottom water, which implies a diffusive flux from pore  
339 waters into bottom waters. The steepest concentration gradients across the sediment-  
340 water interface were observed within the OMZ. The highest Fe(II) concentrations at  
341 the sediment surface (> 6  $\mu\text{M}$ ) occurred at station 4 (145 m water depth). At this station,  
342 the benthic diffusive flux into the bottom waters was also highest with 17.1  $\text{mmol m}^{-2}$   
343  $\text{y}^{-1}$ . The lowest diffusive fluxes of 0.0 (due to concentrations below the detection limit)  
344 and 0.4  $\text{mmol m}^{-2} \text{y}^{-1}$  were observed on the upper slope below the OMZ at stations 9  
345 and 10 respectively (Table 2). An accumulation of  $\text{H}_2\text{S}$  in pore waters coincided with a  
346 depletion of Fe(II) concentrations (Fig. 4). At station 1, we observed the highest  $\text{H}_2\text{S}$   
347 concentrations throughout the core and in particular at the sediment surface, with  
348 maximum concentrations reaching > 4 mM. At stations below the OMZ (stations 9 and  
349 10), no  $\text{H}_2\text{S}$  was detected within pore waters (Fig. 4).

350 Iron concentrations inside the benthic chambers were generally higher than in  
351 ambient bottom waters, and reached maximum values > 300 nM. At stations 4 and 6,  
352 located inside the OMZ, concentrations in the chambers increased in a linear way  
353 during the incubation. At stations above and below the OMZ, we did not observe a  
354 linearly increasing concentration trend over the incubation time. Following previous  
355 studies (Turetta et al., 2005; Severmann et al., 2010; Noffke et al., 2012; Lenstra et al.,  
356 2019) and for comparison with diffusive fluxes, we estimated benthic Fe fluxes from  
357 linear regressions from the change in Fe concentrations in the benthic chamber against  
358 incubation time (Table 2). To test the plausibility of the flux magnitude within the  
359 chamber, we also calculated theoretical concentration gradients over time based on  
360 our diffusive flux estimates (Fig. 5). Our incubation data were largely consistent in  
361 direction and slope with the diffusive benthic fluxes. Especially at stations inside the



362 OMZ (station 4 and 6), where the highest diffusive fluxes of  $17.1$  and  $8.3 \text{ mmol m}^{-2} \text{ y}^{-1}$   
363 were observed, the projected and observed concentration gradients were in good  
364 agreement. At stations below the OMZ, diffusive fluxes of  $< 1 \text{ mmol m}^{-2} \text{ y}^{-1}$  were too  
365 low to be detected over our incubation time of 32 hours.

366

367

### 368 **3.3 Benthic cadmium cycling**

369 In near-bottom waters Cd concentrations increased with distance from the  
370 coast, from  $0.4 \text{ nM}$  at the shallowest station at  $75 \text{ m}$  water depth (station 1) to  $1.1 \text{ nM}$   
371 below the OMZ at  $750 \text{ m}$  water depth (station 9). Cd concentrations were constant  
372 between  $0.5$  and  $4 \text{ m}$  above the seafloor (Fig. 3).

373 Cadmium concentrations in pore waters ranged between  $0.1 - 2 \text{ nM}$  (Fig. 6).  
374 Within the OMZ, bottom water concentrations were higher than concentrations in pore  
375 water within the surface sediments ( $0 - 1 \text{ cm}$ ) indicating a downward diffusive flux into  
376 the sediments. The benthic diffusive fluxes inside the OMZ were of the order of  $0.5 -$   
377  $0.8 \text{ } \mu\text{mol m}^{-2} \text{ y}^{-1}$  (Table 3). In contrast, at station 1 and 9 an upward-directed  
378 concentration gradient was observed, indicating a diffusive flux from the sediments into  
379 bottom waters. The upward diffusive flux ranged from  $1.9$  above the permanent OMZ,  
380 to  $0.2 \text{ } \mu\text{mol m}^{-2} \text{ y}^{-1}$  below the OMZ (Table 3). Pore water Cd concentrations at greater  
381 sediment depths were mostly higher than bottom water concentrations. In some cases  
382 (station 3 and 4), elevated pore water Cd concentrations (up to  $2 \text{ nM}$ ) coincided with  
383 elevated  $\text{H}_2\text{S}$  concentrations (few hundred  $\mu\text{M}$ ).

384 In the benthic chambers three different Cd patterns were observed (Fig. 7).  
385 Above the permanent OMZ (station 1), Cd concentrations in the chambers were low ( $<$   
386  $0.2 \text{ nM}$ ) throughout the incubation period, indicating that there was no Cd flux. At sites  
387 within the OMZ (station 4, 5 and 6), concentrations decreased from  $\sim 0.6 \text{ nM}$  to  $0.3 \text{ nM}$   
388 over the course of the incubation. Below the OMZ (stations 9 and 10), Cd concentration  
389 in the chamber were high ( $\sim 1 \text{ nM}$ ) and remained constant or increased slightly during  
390 the incubation. At sites within the OMZ, Cd removal within the chamber was nearly  
391 linear, which translates to a removal flux of  $13 - 23 \text{ } \mu\text{mol m}^{-2} \text{ y}^{-1}$ . The Cd removal fluxes  
392 in benthic chambers were more than one order of magnitude higher than diffusive  
393 benthic fluxes ( $0.5 - 0.7 \text{ } \mu\text{mol m}^{-2} \text{ y}^{-1}$ ) (Table 3).



394

395

## 396 **4. Discussion**

397

### 398 **4.1 Benthic iron cycling**

#### 399 **4.1.1 Comparison of diffusive and in-situ benthic chamber iron fluxes**

400 In the absence of oxygen and, thus, bottom-dwelling macrofauna at stations  
401 within the OMZ, bioturbation and bioirrigation are unlikely to exert an important control  
402 on sedimentary Fe release. Consistent with this notion, the slope calculated from  
403 benthic diffusive fluxes is largely consistent with the concentration gradients observed  
404 within the benthic chambers (Fig. 5). Moreover, our fluxes from benthic chamber  
405 incubations and diffusive fluxes are generally of the same order of magnitude (few  
406  $\text{mmol m}^{-2} \text{y}^{-1}$ ) (Table 2). Therefore, diffusive transport of dissolved Fe from the  
407 sediment into the bottom water seems to be the main control on the concentration  
408 evolution observed within the benthic chamber.

409 Some of the concentration gradients in benthic chambers are non-linear,  
410 indicating that the Fe flux was not constant during the incubations. This observation  
411 can be used to identify additional processes affecting Fe concentrations and fluxes  
412 within the benthic chamber, which may also affect fluxes under natural conditions. One  
413 possible process that can remove dissolved Fe(II) under anoxic conditions is Fe  
414 oxidation with  $\text{NO}_3^-$  as the terminal electron acceptor or oxidation with  $\text{NO}_2^-$  (Straub et  
415 al., 1996; Carlson et al., 2013; Klueglein and Kappler, 2013). The oxidation of reduced  
416 Fe in the absence of oxygen either biologically mediated by  $\text{NO}_3^-$  or abiotically by  $\text{NO}_2^-$   
417 has been hypothesized to be important in the water column of the Peruvian OMZ  
418 (Scholz et al., 2016; Heller et al., 2017). During our incubation at station 4 (Fig. 8), we  
419 observed a decline in Fe concentrations during the first ten hours of the incubation  
420 time. Concurrently,  $\text{NO}_3^-$  concentrations were decreasing, while  $\text{NO}_2^-$  accumulated,  
421 presumably due to progressive denitrification and release from the sediments. Once  
422  $\text{NO}_3^-$  and  $\text{NO}_2^-$  were quantitatively reduced, Fe concentrations started to rise again and  
423 the following concentration increase resulted in the highest in-situ Fe flux observed  
424 throughout our sampling campaign (Table 2). The coincidence in timing of Fe



425 accumulation and  $\text{NO}_2^-$  decrease suggest that depletion of Fe at the beginning of the  
426 incubation was most likely caused by Fe oxidation with  $\text{NO}_2^-$ . The incubation at station  
427 4 was the only one where  $\text{NO}_3^-$  and  $\text{NO}_2^-$  were quantitatively removed during the  
428 incubation. However, the high Fe flux cannot be interpreted as a natural flux estimate  
429 at steady state. In general, we argue that bottom water  $\text{NO}_2^-$  concentrations exert first  
430 order control on the intensity of Fe efflux at the absence of oxygen and, therefore, need  
431 to be considered in the evaluation of sedimentary Fe mobility in anoxic-nitrogenous  
432 OMZs.

433 During the incubations at the stations 1, 9 and 10, Fe concentrations did not  
434 continuously increase but varied between high and low values. This observation could  
435 be explained by a combination of bioirrigation and bioturbation as well as rapid Fe  
436 oxidation and precipitation. Under oxic conditions, bottom-dwelling macrofauna is likely  
437 to increase the transfer of dissolved Fe from the sediments into the bottom water (Elrod  
438 et al., 2004; Lenstra et al., 2019). During episodes of oxygenation a population of  
439 macrofauna that can enhance bioturbation and bioirrigation was observed on the  
440 Peruvian shelf (Gutiérrez et al., 2008). However, under oxic conditions, any Fe  
441 delivered to the chamber is prone to rapid oxidative removal. Moreover, ex-situ  
442 experiments have demonstrated a fast and efficient removal of up to 90% of dissolved  
443 Fe in incubated bottom waters due to particle resuspension (Homoky et al., 2012).  
444 Interactions with particles and oxidation processes can efficiently remove Fe shortly  
445 after its transfer to bottom waters and this process is likely to be most intense close to  
446 the seafloor where the highest particle concentrations prevail. We argue that the same  
447 processes are reflected by declining Fe concentrations away from seafloor in some of  
448 the bottom water profiles (at station 3 and 4) (Fig. 3).

449

#### 450 **4.1.2 Removal rates of dissolved iron in the benthic boundary layer**

451 We observed declining Fe concentrations in the first 4 m away from the seafloor  
452 at station 3 and 4, which hints at removal of dissolved Fe in the near bottom waters,  
453 after its release from the sediments. To differentiate dilution with ambient bottom water  
454 (by currents) from Fe removal from the dissolved phase, Fe concentrations were  
455 normalized by silicic acid ( $\text{Si}(\text{OH})_4$ ) measured in the same samples (Fig. 3). Due to  
456 opal dissolution within Peru margin sediments, silicic acid is released into bottom  
457 waters (Ehlert et al., 2016). In contrast to Fe, we assume that silicic acid behaves



458 conservatively and precipitation reactions within the bottom waters are of subordinate  
459 importance. The decreasing Fe to Si(OH)<sub>4</sub> ratios at station 3 and 4 with distance from  
460 the seafloor indicate that there is Fe removal within the benthic boundary layer that  
461 must be related to precipitation processes or scavenging.

462 We further constrained rates of dissolved Fe removal at stations with a  
463 discernable Fe to Si(OH)<sub>4</sub> gradient within the first 4 m distance from the seafloor. To  
464 this end, we first determined an eddy diffusion coefficient ( $K_y$ ) using silicic acid fluxes  
465 from benthic chamber incubations ( $F_{Si}$ ) (chapter 2.3 for methodology) and the known  
466 concentration gradient of dissolved silicic acid within the bottom water ( $d_{Si}/d_x$ ), where  
467  $x$  is the height above the seafloor. At the seafloor, the flux of silicic acid from the  
468 sediment is equal to the flux in the water column.

$$469 \quad F_{Si} = -K_y(d_{Si}/d_x) \quad (4)$$

470 This equation can be rearranged to find the eddy diffusion coefficient.

471 Dissolved Fe in the bottom water (DFe) can be described by the following  
472 reaction-transport equation (ignoring advection and assuming a steady-state first-order  
473 consumption of dissolved Fe):

$$474 \quad DFe = C_{BW} * \exp.(-\sqrt{K_{Feox}}/\sqrt{K_y}) \quad (5)$$

475 The equation can be fitted to the measured DFe concentrations in the bottom water by  
476 adjusting the Fe concentration directly above the seafloor ( $C_{BW}$ ) and the Fe oxidation  
477 constant ( $K_{Feox}$ ). From the fitted first-order rate constant  $K_{Feox}$ , we can determine the  
478 half-lives for dissolved Fe in bottom waters.

479 The half-lives of dissolved Fe in the first 4 m away from the seafloor are 2.5 min  
480 and 0.3 min at station 3 and 4, respectively (Table 4). Another study reported a  
481 dissolved Fe half-life of 17 hours under nitrogenous conditions in the first 10 to 20 m  
482 above the seafloor in the Peruvian OMZ (Scholz et al., 2016). Our calculations suggest  
483 that Fe removal in near-bottom waters is much faster. As mentioned above, in the  
484 absence of oxygen, removal processes could be related to oxidation of dissolved Fe  
485 with NO<sub>2</sub><sup>-</sup> or to interactions with suspended particles, which are likely to be most  
486 abundant directly above the seafloor. Further research on dissolved-particulate  
487 interactions in bottom waters is needed to better constrain how sedimentary Fe fluxes  
488 are modified in the benthic boundary layer.



489

#### 490 **4.1.3 Controls on the temporal variability of benthic iron fluxes**

491 The Peruvian OMZ is known to experience high-amplitude fluctuations in  
492 upwelling intensity as well as bottom water oxygen,  $\text{NO}_3^-$ ,  $\text{NO}_2^-$  and  $\text{H}_2\text{S}$  concentrations  
493 (Pennington et al., 2006; Gutiérrez et al., 2008; Graco et al., 2017; Ohde, 2018). To  
494 get an insight into how different biogeochemical conditions control benthic diffusive  
495 Fe(II) fluxes, we compare the fluxes from our recent cruise with fluxes from our earlier  
496 cruise M92 (Fig. 9). Cruise M92 took place in austral autumn 2013 following the main  
497 upwelling season and during a period of intense primary productivity. Due to reduced  
498 upwelling and stable density stratification, the water column on the shallow shelf was  
499 not only depleted in oxygen but also in  $\text{NO}_3^-$  and  $\text{NO}_2^-$  during cruise M92 (Sommer et  
500 al., 2016). Under such conditions, chemolithoautotrophic  $\text{H}_2\text{S}$  oxidation with  $\text{NO}_3^-$  or  
501  $\text{NO}_2^-$  was impeded so that pore water  $\text{H}_2\text{S}$  could be released from the sediment into  
502 the water column. As a result, the water column during M92 was sulfidic between  
503 around 50 and 150 m water depth with the highest  $\text{H}_2\text{S}$  concentration of  $13 \mu\text{M}$   
504 observed at 50 m depth (Fig. 2). While the biogeochemical conditions on the shallow  
505 shelf were fundamentally different to those during M136 and M137, below 150 m water  
506 depth the conditions were largely comparable (oxygen-depleted,  $\text{NO}_3^-$ : 20 – 30  $\mu\text{M}$ ,  
507  $\text{NO}_2^-$  up to 9  $\mu\text{M}$  between 150 – 300 m). At the stations with similar biogeochemical  
508 water column conditions, the Fe(II) fluxes during both our sampling campaigns were  
509 remarkably similar (Fig. 9). However, similar to the temporal variability of Fe  
510 concentrations in bottom waters at station 1 (Fig. 3), we observed a pronounced  
511 difference in the diffusive flux magnitude on the shallow shelf, where the  
512 biogeochemical conditions differed between both cruises. The highest diffusive flux  
513 during M92 in 2013 of  $22.7 \text{ mmol m}^{-2} \text{ y}^{-1}$  was measured at station 1. By contrast, during  
514 M136/137 in 2017 we observed a much lower flux of  $2.6 \text{ mmol m}^{-2} \text{ y}^{-1}$  at this station.  
515 During M136 and M137 the highest flux of  $17.1 \text{ mmol m}^{-2} \text{ y}^{-1}$  was measured at station  
516 4, located at 145 m water depth.

517 Diffusive fluxes are a function of the concentration gradient between pore water  
518 and bottom water (Eq. (1)). As dissolved Fe concentrations in bottom waters are  
519 generally much lower compared to those observed in pore waters, the flux magnitude  
520 is chiefly determined by differences in pore water Fe concentrations. During M92, pore  
521 waters at the sediment surface were characterized by high dissolved Fe concentrations



522 (4.8  $\mu\text{M}$  in the upper pore water), which resulted in a steep gradient and a comparably  
523 high Fe flux. Under the slightly sulfidic conditions that prevailed in the water column  
524 during M92, oxidative removal of dissolved Fe(II) with  $\text{NO}_3^-$  or  $\text{NO}_2^-$  was impeded  
525 (Scholz et al., 2016) and dissolved Fe(II) could be stabilized as aqueous iron sulfide  
526 (Schlosser et al., 2018). Therefore, the bottom water was characterized by high  
527 dissolved Fe concentrations (up to 0.7  $\mu\text{M}$  in MUCs overlying bottom water).

528 Despite oxic conditions in the water column during M136 and M137, we  
529 observed much higher  $\text{H}_2\text{S}$  concentrations in surface sediments at station 1 compared  
530 to M92 (4100  $\mu\text{M}$  during M136 and M137 versus 1800  $\mu\text{M}$  during M92 within the first 8  
531 cm of the core) (Fig. 4). Because of higher  $\text{H}_2\text{S}$  concentrations, Fe concentrations were  
532 controlled by the solubility of Fe monosulfide minerals (FeS). It may seem  
533 counterintuitive that the surface sediment was highly sulfidic, while the overlying water  
534 column was oxygenated. In order to explain this observation, we need to consider the  
535 role of mats of filamentous sulfur oxidizing bacteria in controlling  $\text{H}_2\text{S}$  concentrations  
536 in surface sediments. (Gutiérrez et al., 2008; Noffke et al., 2012; Yücel et al., 2017).  
537 During M92 these mats were generally abundant on the shelf and upper slope, thus  
538 limiting the extent of  $\text{H}_2\text{S}$  accumulation within surface sediments (Sommer et al., 2016).  
539 Previous studies demonstrated that mats of sulfur oxidizing bacteria can disappear  
540 during periods of oxygenation (Gutiérrez et al., 2008). Consistent with this previous  
541 finding, visual inspection of the seafloor using the video-guided MUC revealed that the  
542 abundance of bacterial mats on the seafloor seemed greatly reduced, which is most  
543 probably related to oxic bottom water conditions on the shallow shelf during the coastal  
544 El Niño event. As these microaerophilic organisms tend to avoid high oxygen  
545 concentrations they probably started to withdraw into the sediment once oxygen levels  
546 raised. Furthermore, an abundance of red squat lobster (*Pleuroncodes monodon*),  
547 which are known to feed on bacterial mats (Gallardo et al., 1994), was observed at the  
548 seafloor on the shallow shelf. We suggest that the retreat of sulfide-oxidizing bacteria  
549 under oxic conditions created a situation where  $\text{H}_2\text{S}$  accumulation in the surface  
550 sediment and FeS precipitation limited the extent of Fe release into the bottom water.

551

## 552 **4.2 Benthic cadmium cycling**

### 553 **4.2.1 Comparison of diffusive and in-situ benthic chamber cadmium fluxes**



554 At stations above the permanent and below the OMZ (stations 1, 9 and 10),  
555 diffusive Cd fluxes and fluxes in benthic chambers were largely consistent (Table 3).  
556 In contrast, the fluxes determined with benthic chambers at stations within the OMZ  
557 (station 4, 5 and 6) were 25 to 40 times higher than the diffusive flux (Table 3). This  
558 discrepancy demonstrates that diffusion cannot be the dominant process leading to  
559 the continuous decrease of dissolved Cd during benthic chamber incubations.  
560 Alternatively, Cd could be precipitated within the benthic chamber and removed  
561 through downward sinking of Cd-rich particles. Cadmium sulfide (greenockite) has a  
562 relatively low solubility compared to sulfide minerals of other TMs (solubility product of  
563  $\text{CdS} = -16.4 \ll \text{FeS} = -3.9$ ). It is generally agreed that CdS precipitation can take  
564 place at trace amounts of  $\text{H}_2\text{S}$  ( $\text{H}_2\text{S} < 1 \mu\text{M}$ , i.e., below the detection limit of the method  
565 applied in this study) (Davies-Colley et al., 1985; Rosenthal et al., 1995). Previous  
566 studies using in-situ benthic flux chambers have concluded that production of  $\text{H}_2\text{S}$  in  
567 the sediment or the accumulation of  $\text{H}_2\text{S}$  in benthic chambers during incubations can  
568 switch the direction of the Cd flux or intensify Cd removal through CdS precipitation  
569 (Westerlund et al., 1986; Colbert et al., 2001). Precipitation of CdS during the  
570 incubation is, therefore, a viable explanation for the discrepancy between diffusive Cd  
571 flux and Cd fluxes in benthic chambers observed in our study. Furthermore, the three  
572 different pattern of Cd concentration trends observed in benthic chamber incubations  
573 can be related to  $\text{H}_2\text{S}$  concentrations in the surface sediment below the benthic  
574 chambers (Table 3). At stations within the OMZ, pore water  $\text{H}_2\text{S}$  concentrations in  
575 surface sediments were moderate (few  $\mu\text{M}$ ). It is likely that there was a continuous  
576 leakage of trace amounts of  $\text{H}_2\text{S}$  from the pore water into the incubated bottom waters  
577 during the incubation thus leading to CdS precipitation and declining Cd  
578 concentrations. On the shallowest shelf station, where pore water  $\text{H}_2\text{S}$  concentrations  
579 in the surface sediment were high (hundreds of  $\mu\text{M}$ ), a potentially large amount could  
580 have been released at the beginning of the incubation thus explaining pronounced Cd  
581 depletion in the chamber compared to the surrounding bottom water (0.1 nM within the  
582 chamber compared to 0.4 nM outside the chamber). Below the OMZ, where there was  
583 no  $\text{H}_2\text{S}$  present in surface sediments, there was no Cd depletion in the chamber during  
584 the incubation and, consistent with previous studies in oxic settings (Westerlund et al.,  
585 1986; Ciceri et al., 1992; Zago et al., 2000; Turetta et al., 2005), both diffusive and  
586 benthic chamber flux data were indicative of an upward-directed flux out of the  
587 sediment. Due to the absence of  $\text{H}_2\text{S}$ , dissolved Cd released from biogenic particles in



588 the surface sediment could accumulate in the pore water thus driving a diffusive flux  
589 out of the sediment.

590

#### 591 **4.2.2 Quantification of the sedimentary cadmium sink**

592 Consistent with our Cd flux data there is general consent that OMZs are a sink  
593 for Cd. Several water column studies have observed Cd depletion in water masses  
594 within the Peruvian and other OMZs, which was mostly attributed to Cd removal via  
595 CdS precipitation in sulfidic micro-niches within particles in the water column (Janssen  
596 et al., 2014; Conway and John, 2015b; Xie et al., 2019). Sedimentary studies showed  
597 that Cd is highly enriched in OMZ sediments, which has mostly been attributed to the  
598 delivery of Cd with organic material and subsequent fixation as CdS within sulfidic  
599 sediments (Ragueneau et al., 2000; Böning et al., 2004; Borchers et al., 2005; Muñoz  
600 et al., 2012; Little et al., 2015). Based on our data, we can quantify the delivery of Cd  
601 to the sediments via three different pathways: (1) diffusion across the sediment-water  
602 interface and CdS precipitation within the sediment; (2) Cd incorporation by  
603 phytoplankton and delivery to the sediment with organic matter; (3) CdS precipitation  
604 in the water column and particulate delivery to the sediment (Table 3).

605 The enrichment of Cd in the sediment relative to the lithogenic background  
606 (expressed as excess Cd concentration,  $Cd_{xs}$ ) was calculated using the following  
607 equation (Brumsack, 2006):

$$608 \quad Cd_{xs} = Cd_{sample} - Al_{sample} * (Cd/Al)_{crust} \quad (6)$$

609 The Cd/Al ratio of the upper continental crust ( $1.22 \cdot 10^{-6}$ ) was used as lithogenic  
610 background reference (Taylor and McLennan, 2009). To get a flux of Cd to the  
611 sediment,  $Cd_{xs}$  was multiplied with the mass accumulation rate (MAR) from published  
612 data for each individual site (Dale et al., 2015b). To approximate the amount of Cd  
613 delivered to the sediment with organic material, the average concentration ratio of Cd  
614 to C in phytoplankton (Moore et al., 2013) was multiplied by published particulate  
615 organic carbon rain rates (maximum estimate) or burial rates (minimum estimate) for  
616 each individual site (Dale et al., 2015b). The Cd delivery via precipitation in the water  
617 column was determined as the remainder of  $Cd_{xs} * MAR$  after subtraction of the two  
618 other sources (i.e., diffusive flux and delivery by organic material).



619 Sediments at all stations on the Peruvian shelf and slope are enriched in Cd  
620 relative to the lithogenic background. The accumulation rate of  $Cd_{xs}$  decreases from  
621  $250 \mu\text{mol m}^{-2} \text{y}^{-1}$  at the station 1 at 75 m to  $4 \mu\text{mol m}^{-2} \text{y}^{-1}$  at station 9 at 750 m water  
622 depth (Table 3). These fluxes generally exceed the amount of Cd delivered to the  
623 sediments via diffusion and associated with organic material. Together these  
624 mechanisms of Cd delivery can only account for  $\sim 20\%$  of the  $Cd_{xs}$  at stations above  
625 and inside the OMZ, with the delivery with organic material being of greater importance.  
626 The remaining water column Cd removal ( $\sim 80\%$ ) must be related to CdS precipitation  
627 in the water column and delivery of Cd-rich particles to the sediment. This removal  
628 process can be a combination of precipitation in sulfidic micro-niches around sinking  
629 particles (Janssen et al., 2014; Bianchi et al., 2018), CdS precipitation in sulfide plumes  
630 (Xie et al., 2019) when sedimentary  $\text{H}_2\text{S}$  can spread throughout the water column  
631 (Schunck et al., 2013; Ohde, 2018), and precipitation of CdS in the near-bottom water  
632 (this study). Our estimated CdS precipitation in the water column within the OMZ agree  
633 with the Cd fluxes we determined from benthic chamber incubations, where dissolved  
634 Cd removal takes place in the first 20 cm – 30 cm away from the sediment surface.  
635 These Cd removal fluxes alone are sufficient to account for 41% – 68% of the  
636 estimated particulate Cd removal from the water column and 38% - 60% of total  $Cd_{xs}$   
637 in the sediment within the OMZ (Table 3). Considering that Cd precipitation in near-  
638 bottom water is unlikely to be restricted to the 20 – 30 cm above the seafloor covered  
639 by our benthic chambers, the removal flux associated with this process is likely to be  
640 even higher. Below the OMZ at 750 m, where the smallest Cd enrichment is observed,  
641 the relative contribution of Cd delivery with organic material increases. About half of  
642 the  $Cd_{xs}$  can derive from organic material at this station.

643 Once Cd is delivered to the sediment it can either stay fixed in the solid phase  
644 or it can be released into the pore waters. Cadmium concentrations in pore waters of  
645 subsurface sediments ( $> 10$  cm sediment depth) were mostly higher than bottom water  
646 concentrations (Fig. 6), indicating a transfer of Cd from the solid phase into pore waters  
647 during early diagenesis. Cadmium sulfides are considered highly insoluble and stable  
648 within sediments (Elderfield et al., 1981), even upon re-oxygenation (Rosenthal et al.,  
649 1995). Therefore, Cd release through re-dissolution of CdS is ruled out as a potential  
650 source of dissolved Cd. Alternatively, Cd liberation upon remineralization of organic  
651 material could explain elevated Cd concentrations in the pore water. Elevated Cd  
652 concentrations in sulfidic pore waters have been observed in previous studies and



653 attributed to Cd stabilization through formation of organic and inorganic complexes  
654 (Gobeil et al., 1987; Sundby et al., 2004). Experimental data gave evidence for the  
655 presence of dissolved Cd bisulfide and polysulfide complexes in pore waters. An  
656 increase of electrochemically active Cd after UV irradiation, was explained by the  
657 destruction of electrochemically inactive bisulfide and polysulfide complexes (Gobeil et  
658 al., 1987). At very high H<sub>2</sub>S concentrations (> 10<sup>-3</sup> M) the solubility of Cd may increase  
659 due to an increase in these bisulfide and polysulfide complexes. Under such highly  
660 sulfidic conditions, Cd solubility may even exceed the solubility in oxygenated waters  
661 and highly sulfidic sediment can eventually turn into a diffusive source of Cd to the  
662 bottom water (Davies-Colley et al., 1985). Such a scenario can explain the negative  
663 (i.e., upward-directed) diffusive Cd flux at station 1, where the pore waters of surface  
664 sediments are highly sulfidic.

665

666

## 667 **5. Conclusions and implications for trace metal sources and sinks in the future** 668 **ocean**

669 Consistent with earlier work, our results demonstrate that that OMZ sediments  
670 are a source for Fe and a sink for Cd. Moreover, our findings allow to further constrain  
671 the different biogeochemical conditions and processes that control the benthic fluxes  
672 of these TM across the Peruvian OMZ.

673 Iron is transported via diffusion from the sediment pore water into bottom water.  
674 The accumulation of high levels of H<sub>2</sub>S in pore waters, modulated by the abundance  
675 of sulfur oxidizing bacteria, can reduce diffusive Fe release through sulfide precipitation  
676 within pore waters. In anoxic bottom waters Fe can be rapidly removed, likely via  
677 oxidation by NO<sub>2</sub><sup>-</sup> and/or interaction with particles. Benthic Cd fluxes are directed from  
678 the bottom water into the sediment within the OMZ. Diffusive fluxes and delivery of Cd  
679 via organic material cannot account for the sedimentary Cd enrichment. Instead CdS  
680 precipitation in near bottom waters could be the most important pathway that delivers  
681 Cd to the sediments.

682 According to our results, H<sub>2</sub>S concentrations in surface sediments exert a first  
683 order control on the magnitude and direction of Fe and Cd fluxes across the sediment-  
684 water interface. With generally decreasing oxygen concentrations in the ocean and an



685 expansion of OMZs (Stramma et al., 2008; Schmidtko et al., 2017), sulfidic surface  
686 sediments will likely also expand. With regard to the solubility of their sulfide minerals,  
687 Fe and Cd represent two opposite end members. The solubility of sulfide minerals of  
688 other important nutrient-type TMs, such as Ni and Zn, is intermediate between those  
689 of Fe and Cd ( $Fe > Ni > Zn > Cd$ ). An expansion of sulfidic surface sediments is thus  
690 likely to affect sedimentary TM fluxes in a differing manner. This notion is illustrated in  
691 Fig. 10, showing saturation indices calculated based on the range of TM  
692 concentrations observed in the ocean and typical  $H_2S$  concentrations observed in  
693 anoxic marine environments (nM -  $\mu M$  concentrations represent sulfidic events in the  
694 water column, pore water conditions are represented by up  $\mu M$  - mM concentrations).  
695 Cadmium sulfide minerals become oversaturated at nM to  $\mu M$   $H_2S$  concentrations,  
696 which is why Cd removal can take place in the bottom water in OMZs. By contrast, FeS  
697 is highly undersaturated under the typical biogeochemical conditions in the water  
698 column. Therefore, FeS precipitation is unlikely to take place in the water column, even  
699 under somewhat more reducing conditions. Other sulfide-forming TMs have an  
700 intermediate sulfide solubility, which could imply that the direction and magnitude of  
701 their sedimentary fluxes is susceptible to expanding ocean anoxia. The differing  
702 response of TMs to an expansion of sulfidic conditions may cause a change in the TM  
703 stoichiometry of upwelling water masses with potential consequences for TM-  
704 dependent marine ecosystems in surface waters.

705

706

#### 707 **Data availability**

708 The data will be made available at Pangaea upon publication of the article.

709

710

#### 711 **Author contribution**

712 AP and FS conceived the study. AP, FS, AD, SS conducted the sampling at sea. AP  
713 analyzed the trace metal concentrations. AP and FS prepared the manuscript with  
714 contributions from all co-authors.

715



716

717 **Competing Interests**

718 The authors declare that they have no conflict of interest.

719

720

721 **Acknowledgements**

722 We are grateful for the support of the crew of RV Meteor during the fieldwork. For their  
723 technical and analytical assistance we thank A. Beck, A. Bleyer, B. Domeyer, A.  
724 Petersen, T. Steffens, R. Surberg and M. Türck. This study was supported by the  
725 German Research Foundation through the Emmy Noether Nachwuchsforschergruppe  
726 ICONOX (Iron Cycling in Continental Margin Sediments and the Nutrient and Oxygen  
727 Balance of the Ocean) and Sonderforschungsbereich 754 (Climate-Biogeochemistry  
728 Interactions in the Tropical Ocean).



729 **References**

730

731 Audry, S., Blanc, G., Schäfer, J., Chaillou, G. and Robert, S.: Early diagenesis of  
732 trace metals (Cd, Cu, Co, Ni, U, Mo, and V) in the freshwater reaches of a macrotidal  
733 estuary, *Geochim. Cosmochim. Acta*, 70(9), 2264–2282,  
734 doi:10.1016/j.gca.2006.02.001, 2006.

735 Bianchi, D., Weber, T. S., Kiko, R. and Deutsch, C.: Global niche of marine anaerobic  
736 metabolisms expanded by particle microenvironments, *Nat. Geosci.*, 11(April), 1–6,  
737 doi:10.1038/s41561-018-0081-0, 2018.

738 Biller, D. V. and Bruland, K. W.: Sources and distributions of Mn, Fe, Co, Ni, Cu, Zn,  
739 and Cd relative to macronutrients along the central California coast during the spring  
740 and summer upwelling season, *Mar. Chem.*, 155, 50–70,  
741 doi:10.1016/j.marchem.2013.06.003, 2013.

742 Böning, P., Brumsack, H. J., Böttcher, M. E., Schnetger, B., Kriete, C., Kallmeyer, J.  
743 and Borchers, S. L.: Geochemistry of Peruvian near-surface sediments, *Geochim.  
744 Cosmochim. Acta*, 68(21), 4429–4451, doi:10.1016/j.gca.2004.04.027, 2004.

745 Bopp, L., Le Quéré, C., Heimann, M., Manning, A. C. and Monfray, P.: Climate-  
746 induced oceanic oxygen fluxes: Implications for the contemporary carbon budget,  
747 *Global Biogeochem. Cycles*, 16(2), 6-1-6–13, doi:10.1029/2001GB001445, 2002.

748 Borchers, S. L., Schnetger, B., Böning, P. and Brumsack, H.-J.: Geochemical  
749 signatures of the Namibian diatom belt: Perennial upwelling and intermittent anoxia,  
750 *Geochemistry, Geophys. Geosystems*, 6(6), doi:10.1029/2004GC000886, 2005.

751 Boudreau, B. P.: *Diagenetic Models and Their Implementation*, Springer., 1997.

752 Boyd, P. W. and Ellwood, M. J.: The biogeochemical cycle of iron in the ocean, *Nat.  
753 Geosci.*, 3(10), 675–682, doi:10.1038/ngeo964, 2010.

754 Bruland, K. W. and Lohan, M. C.: Controls of Trace Metals in Seawater, in *Treatise  
755 on Geochemistry*, pp. 23–47, Elsevier., 2003.

756 Brumsack, H. J.: The trace metal content of recent organic carbon-rich sediments:  
757 Implications for Cretaceous black shale formation, *Palaeogeogr. Palaeoclimatol.  
758 Palaeoecol.*, 232(2–4), 344–361, doi:10.1016/j.palaeo.2005.05.011, 2006.



- 759 Canfield, D. E.: Reactive iron in marine sediments, *Geochim. Cosmochim. Acta*,  
760 53(3), 619–632, doi:10.1016/0016-7037(89)90005-7, 1989.
- 761 Carlson, H. K., Clark, I. C., Blazewicz, S. J., Iavarone, A. T. and Coates, J. D.: Fe(II)  
762 Oxidation Is an Innate Capability of Nitrate-Reducing Bacteria That Involves Abiotic  
763 and Biotic Reactions, *J. Bacteriol.*, 195(14), 3260–3268, doi:10.1128/JB.00058-13,  
764 2013.
- 765 Ciceri, G., Maran, C., Martinotti, W. and Queirazza, G.: Geochemical cycling of heavy  
766 metals in a marine coastal area: benthic flux determination from pore water profiles  
767 and in situ measurements using benthic chambers, *Hydrobiologia*, 235–236(1), 501–  
768 517, doi:10.1007/BF00026238, 1992.
- 769 Colbert, D., Coale, K. ., Berelson, W. . and Johnson, K. .: Cadmium Flux in Los  
770 Angeles/Long Beach Harbours and at Sites along the California Continental Margin,  
771 *Estuar. Coast. Shelf Sci.*, 53(2), 169–180, doi:10.1006/ecss.2001.0802, 2001.
- 772 Collier, R. and Edmond, J.: The trace element geochemistry of marine biogenic  
773 particulate matter, *Prog. Oceanogr.*, 13(2), 113–199, doi:10.1016/0079-  
774 6611(84)90008-9, 1984.
- 775 Conway, T. M. and John, S. G.: Quantification of dissolved iron sources to the North  
776 Atlantic Ocean, *Nature*, 511(7508), 212–215, doi:10.1038/nature13482, 2014.
- 777 Conway, T. M. and John, S. G.: Biogeochemical cycling of cadmium isotopes along a  
778 high-resolution section through the North Atlantic Ocean, *Geochim. Cosmochim.*  
779 *Acta*, 148, 269–283, doi:10.1016/j.gca.2014.09.032, 2015a.
- 780 Conway, T. M. and John, S. G.: The cycling of iron, zinc and cadmium in the North  
781 East Pacific Ocean - Insights from stable isotopes, *Geochim. Cosmochim. Acta*, 164,  
782 262–283, doi:10.1016/j.gca.2015.05.023, 2015b.
- 783 Dale, A. W., Nickelsen, L., Scholz, F., Hensen, C., Oeschlies, A. and Wallmann, K.: A  
784 revised global estimate of dissolved iron fluxes from marine sediments, *Global*  
785 *Biogeochem. Cycles*, 29(5), 691–707, doi:10.1002/2014GB005017, 2015a.
- 786 Dale, A. W., Sommer, S., Lomnitz, U., Montes, I., Treude, T., Liebetrau, V., Gier, J.,  
787 Hensen, C., Dengler, M., Stolpovsky, K., Bryant, L. D. and Wallmann, K.: Organic  
788 carbon production, mineralisation and preservation on the Peruvian margin,  
789 *Biogeosciences*, 12(5), 1537–1559, doi:10.5194/bg-12-1537-2015, 2015b.



- 790 Dalsgaard, T., Thamdrup, B., Farías, L. and Revsbech, N. P.: Anammox and  
791 denitrification in the oxygen minimum zone of the eastern South Pacific, *Limnol.*  
792 *Oceanogr.*, 57(5), 1331–1346, doi:10.4319/lo.2012.57.5.1331, 2012.
- 793 Davies-Colley, R. J., Nelson, P. O. and Williamson, K. J.: Sulfide control of cadmium  
794 and copper concentrations in anaerobic estuarine sediments, *Mar. Chem.*, 16(2),  
795 173–186, doi:10.1016/0304-4203(85)90021-0, 1985.
- 796 Echevin, V., Colas, F., Espinoza-Morriberon, D., Vasquez, L., Anculle, T. and  
797 Gutierrez, D.: Forcings and Evolution of the 2017 Coastal El Niño Off Northern Peru  
798 and Ecuador, *Front. Mar. Sci.*, 5(October), 1–16, doi:10.3389/fmars.2018.00367,  
799 2018.
- 800 Ehlert, C., Doering, K., Wallmann, K., Scholz, F., Sommer, S., Grasse, P., Geilert, S.  
801 and Frank, M.: Stable silicon isotope signatures of marine pore waters – Biogenic  
802 opal dissolution versus authigenic clay mineral formation, *Geochim. Cosmochim.*  
803 *Acta*, 191, 102–117, doi:10.1016/j.gca.2016.07.022, 2016.
- 804 Elderfield, H., McCaffrey, R. J., Luedtke, N., Bender, M. and Truesdale, V. W.:  
805 Chemical diagenesis in Narragansett Bay sediments, *Am. J. Sci.*, 281(8), 1021–1055,  
806 doi:10.2475/ajs.281.8.1021, 1981.
- 807 Elrod, V. A., Berelson, W. M., Coale, K. H. and Johnson, K. S.: The flux of iron from  
808 continental shelf sediments: A missing source for global budgets, *Geophys. Res.*  
809 *Lett.*, 31(12), n/a-n/a, doi:10.1029/2004GL020216, 2004.
- 810 Fitzsimmons, J. N., Conway, T. M., Lee, J.-M., Kayser, R., Thyng, K. M., John, S. G.  
811 and Boyle, E. A.: Dissolved iron and iron isotopes in the southeastern Pacific Ocean,  
812 *Global Biogeochem. Cycles*, 30(10), 1372–1395, doi:10.1002/2015GB005357, 2016.
- 813 Gallardo, V. A., Cañete, J. I., Roa, R., Enríquez-Briones, S. and Baltazar, M.:  
814 Recruitment of the Squat Lobster Pleuroncodes Monodon on the Continental Shelf  
815 Off Central Chile, , 14(4), doi:10.1163/193724094X00632, 1994.
- 816 Garreaud, R. D.: A plausible atmospheric trigger for the 2017 coastal El Niño, *Int. J.*  
817 *Climatol.*, 38(January 2017), e1296–e1302, doi:10.1002/joc.5426, 2018.
- 818 Gendron, A., Silverberg, N., Sundby, B. and Lebel, J.: Early diagenesis of cadmium  
819 and cobalt in sediments of the Laurentian Trough, *Geochim. Cosmochim. Acta*,  
820 50(5), 741–747, doi:10.1016/j.jmactools.2007.10.013, 1986.



- 821 Gerringa, L. J. A.: Aerobic degradation of organic matter and the mobility of Cu, Cd,  
822 Ni, Pb, Zn, Fe and Mn in marine sediment slurries, *Mar. Chem.*, 29(C), 355–374,  
823 doi:10.1016/0304-4203(90)90023-6, 1990.
- 824 Gobeil, C., Silverberg, N., Sundby, B. and Cossa, D.: Cadmium diagenesis in  
825 Laurentian Trough sediments, *Geochim. Cosmochim. Acta*, 51(3), 589–596,  
826 doi:10.1016/0016-7037(87)90071-8, 1987.
- 827 Graco, M. I., Purca, S., Dewitte, B., Castro, C. G., Morón, O., Ledesma, J., Flores, G.  
828 and Gutiérrez, D.: The OMZ and nutrient features as a signature of interannual and  
829 low-frequency variability in the Peruvian upwelling system, *Biogeosciences*, 14(20),  
830 4601–4617, doi:10.5194/bg-14-4601-2017, 2017.
- 831 Grasshoff, M., Erhardt, M. and Kremling, K.: *Methods of seawater analysis.*, Wiley-  
832 VCH, Weinheim, doi:10.1002/ange.19770890738, 1999.
- 833 Gutiérrez, D., Enríquez, E., Purca, S., Quipúzcoa, L., Marquina, R., Flores, G. and  
834 Graco, M.: Oxygenation episodes on the continental shelf of central Peru: Remote  
835 forcing and benthic ecosystem response, *Prog. Oceanogr.*, 79(2–4), 177–189,  
836 doi:10.1016/j.pocean.2008.10.025, 2008.
- 837 Hawco, N. J., Ohnemus, D. C., Resing, J. A., Twining, B. S. and Saito, M. A.: A  
838 dissolved cobalt plume in the oxygen minimum zone of the eastern tropical South  
839 Pacific, *Biogeosciences*, 13(20), 5697–5717, doi:10.5194/bg-13-5697-2016, 2016.
- 840 Heller, M. I., Lam, P. J., Moffett, J. W., Till, C. P., Lee, J. M., Toner, B. M. and  
841 Marcus, M. A.: Accumulation of Fe oxyhydroxides in the Peruvian oxygen deficient  
842 zone implies non-oxygen dependent Fe oxidation, *Geochim. Cosmochim. Acta*, 211,  
843 174–193, doi:10.1016/j.gca.2017.05.019, 2017.
- 844 Helm, K. P., Bindoff, N. L. and Church, J. A.: Observed decreases in oxygen content  
845 of the global ocean, *Geophys. Res. Lett.*, 38(23), 1–6, doi:10.1029/2011GL049513,  
846 2011.
- 847 Homoky, W. B., Severmann, S., McManus, J., Berelson, W. M., Riedel, T. E.,  
848 Statham, P. J. and Mills, R. A.: Dissolved oxygen and suspended particles regulate  
849 the benthic flux of iron from continental margins, *Mar. Chem.*, 134–135, 59–70,  
850 doi:10.1016/j.marchem.2012.03.003, 2012.
- 851 Hydes, D., Aoyama, M., Aminot, A., Bakker, K., Becker, S., Coverly, S., Daniel, A.,



- 852 Dickson, A. G., Grosso, O., Kerouel, R., van Ooijen, J., Sato, K., Tanhua, T.,  
853 Woodward, E. M. S. and Zhang, J. Z.: Determination of dissolved nutrients (N, P, Si)  
854 in seawater with high precision and inter-comparability using gas-segmented  
855 continuous flow analysers, Go-sh. Repeat Hydrogr. Man. IOCCP Rep. A Collect.  
856 Expert Reports Guidel., 134(14), 1–87 [online] Available from:  
857 <http://archimer.ifremer.fr/doc/00020/13141/>, 2010.
- 858 Janssen, D. J., Conway, T. M., John, S. G., Christian, J. R., Kramer, D. I., Pedersen,  
859 T. F. and Cullen, J. T.: Undocumented water column sink for cadmium in open ocean  
860 oxygen-deficient zones, *Proc. Natl. Acad. Sci.*, 111(19), 6888–6893,  
861 doi:10.1073/pnas.1402388111, 2014.
- 862 John, S. G., Helgoe, J., Townsend, E., Weber, T., DeVries, T., Tagliabue, A., Moore,  
863 K., Lam, P., Marsay, C. M. and Till, C.: Biogeochemical cycling of Fe and Fe stable  
864 isotopes in the Eastern Tropical South Pacific, *Mar. Chem.*, 201(March), 66–76,  
865 doi:10.1016/j.marchem.2017.06.003, 2018.
- 866 Karstensen, J., Stramma, L. and Visbeck, M.: Oxygen minimum zones in the eastern  
867 tropical Atlantic and Pacific oceans, *Prog. Oceanogr.*, 77(4), 331–350,  
868 doi:10.1016/j.pocean.2007.05.009, 2008.
- 869 Keeling, R. F., Körtzinger, A. and Gruber, N.: Ocean Deoxygenation in a Warming  
870 World, *Ann. Rev. Mar. Sci.*, 2(1), 199–229,  
871 doi:10.1146/annurev.marine.010908.163855, 2010.
- 872 Klar, J. K., Schlosser, C., Milton, J. A., Woodward, E. M. S., Lacan, F., Parkinson, I.  
873 J., Achterberg, E. P. and James, R. H.: Sources of dissolved iron to oxygen minimum  
874 zone waters on the Senegalese continental margin in the tropical North Atlantic  
875 Ocean: Insights from iron isotopes, *Geochim. Cosmochim. Acta*, 236, 60–78,  
876 doi:10.1016/j.gca.2018.02.031, 2018.
- 877 Klinkhammer, G., Heggie, D. T. and Graham, D. W.: Metal diagenesis in oxic marine  
878 sediments, *Earth Planet. Sci. Lett.*, 61(2), 211–219, doi:10.1016/0012-  
879 821X(82)90054-1, 1982.
- 880 Klueglein, N. and Kappler, A.: Abiotic oxidation of Fe(II) by reactive nitrogen species  
881 in cultures of the nitrate-reducing Fe(II) oxidizer *Acidovorax* sp. BoFeN1 - questioning  
882 the existence of enzymatic Fe(II) oxidation, *Geobiology*, 11(2), 180–190,



- 883 doi:10.1111/gbi.12019, 2013.
- 884 Lam, P. and Kuypers, M. M. M.: Microbial Nitrogen Cycling Processes in Oxygen  
885 Minimum Zones, *Ann. Rev. Mar. Sci.*, 3(1), 317–345, doi:10.1146/annurev-marine-  
886 120709-142814, 2011.
- 887 Lam, P., Lavik, G., Jensen, M. M., van de Vossenberg, J., Schmid, M., Woebken, D.,  
888 Gutierrez, D., Amann, R., Jetten, M. S. M. and Kuypers, M. M. M.: Revising the  
889 nitrogen cycle in the Peruvian oxygen minimum zone, *Proc. Natl. Acad. Sci.*, 106(12),  
890 4752–4757, doi:10.1073/pnas.0812444106, 2009.
- 891 Lane, T. W. and Morel, F. M. M.: A biological function for cadmium in marine diatoms,  
892 *Proc. Natl. Acad. Sci.*, 97(9), 4627–4631, doi:10.1073/pnas.090091397, 2000.
- 893 Lee, J. and Morel, F.: Replacement of zinc by cadmium in marine phytoplankton,  
894 *Mar. Ecol. Prog. Ser.*, 127(1–3), 305–309, doi:10.3354/meps127305, 1995.
- 895 Lenstra, W. K., Hermans, M., Séguret, M. J. M., Witbaard, R., Behrends, T., Dijkstra,  
896 N., van Helmond, N. A. G. M., Kraal, P., Laan, P., Rijkenberg, M. J. A., Severmann,  
897 S., Teacă, A. and Slomp, C. P.: The shelf-to-basin iron shuttle in the Black Sea  
898 revisited, *Chem. Geol.*, 511(April), 314–341, doi:10.1016/j.chemgeo.2018.10.024,  
899 2019.
- 900 Levin, L., Gutiérrez, D., Rathburn, A., Neira, C., Sellanes, J., Muñoz, P., Gallardo, V.  
901 and Salamanca, M.: Benthic processes on the Peru margin: a transect across the  
902 oxygen minimum zone during the 1997–98 El Niño, *Prog. Oceanogr.*, 53(1), 1–27,  
903 doi:10.1016/S0079-6611(02)00022-8, 2002.
- 904 Li, Y.-H. and Gregory, S.: Diffusion of ions in sea water and in deep-sea sediments,  
905 *Geochim. Cosmochim. Acta*, 38(5), 703–714, doi:10.1016/0016-7037(74)90145-8,  
906 1974.
- 907 Little, S. H., Vance, D., Lyons, T. W. and McManus, J.: Controls on trace metal  
908 authigenic enrichment in reducing sediments: Insights from modern oxygen-deficient  
909 settings, *Am. J. Sci.*, 315(2), 77–119, doi:10.2475/02.2015.01, 2015.
- 910 Liu, X. and Millero, F. J.: The solubility of iron in seawater, *Mar. Chem.*, 77(1), 43–54,  
911 doi:10.1016/S0304-4203(01)00074-3, 2002.
- 912 Lohan, M. C. and Bruland, K. W.: Elevated Fe(II) and dissolved Fe in hypoxic shelf



- 913 waters off Oregon and Washington: An enhanced source of iron to coastal upwelling  
914 regimes, *Environ. Sci. Technol.*, 42(17), 6462–6468, doi:10.1021/es800144j, 2008.
- 915 Lüdke, J., Dengler, M., Sommer, S., Clemens, D., Thomsen, S., Krahmann, G., Dale,  
916 A. W., Achterberg, E. P. and Visbeck, M.: Influence of intraseasonal eastern  
917 boundary circulation variability on hydrography and biogeochemistry off Peru, *Ocean*  
918 *Sci. Discuss.*, 1(August), 1–31, doi:10.5194/os-2019-93, 2019.
- 919 Moore, C. M., Mills, M. M., Arrigo, K. R., Berman-Frank, I., Bopp, L., Boyd, P. W.,  
920 Galbraith, E. D., Geider, R. J., Guieu, C., Jaccard, S. L., Jickells, T. D., La Roche, J.,  
921 Lenton, T. M., Mahowald, N. M., Marañón, E., Marinov, I., Moore, J. K., Nakatsuka,  
922 T., Oeschies, A., Saito, M. A., Thingstad, T. F., Tsuda, A. and Ulloa, O.: Processes  
923 and patterns of oceanic nutrient limitation, *Nat. Geosci.*, 6(9), 701–710,  
924 doi:10.1038/ngeo1765, 2013.
- 925 Morel, F. M. M., Milligan, A. J. and Saito, M. A.: Marine Bioinorganic Chemistry: The  
926 Role of Trace Metals in the Oceanic Cycles of Major Nutrients, in *Treatise on*  
927 *Geochemistry*, vol. 197, pp. 123–150, Elsevier., 2014.
- 928 Morse, J. W. and Luther, G. W.: Chemical influences on trace metal-sulfide  
929 interactions in anoxic sediments, *Geochim. Cosmochim. Acta*, 63(19–20), 3373–  
930 3378, doi:10.1016/S0016-7037(99)00258-6, 1999.
- 931 Muñoz, P., Dezileau, L., Cardenas, L., Sellanes, J., Lange, C. B., Inostroza, J.,  
932 Muratli, J. and Salamanca, M. A.: Geochemistry of trace metals in shelf sediments  
933 affected by seasonal and permanent low oxygen conditions off central Chile, SE  
934 Pacific (~36°S), *Cont. Shelf Res.*, 33, 51–68, doi:10.1016/j.csr.2011.11.006, 2012.
- 935 Noble, A. E., Lamborg, C. H., Ohnemus, D. C., Lam, P. J., Goepfert, T. J., Measures,  
936 C. I., Frame, C. H., Casciotti, K. L., DiTullio, G. R., Jennings, J. and Saito, M. A.:  
937 Basin-scale inputs of cobalt, iron, and manganese from the Benguela-Angola front to  
938 the South Atlantic Ocean, *Limnol. Oceanogr.*, 57(4), 989–1010,  
939 doi:10.4319/lo.2012.57.4.0989, 2012.
- 940 Noffke, A., Hensen, C., Sommer, S., Scholz, F., Bohlen, L., Mosch, T., Graco, M. and  
941 Wallmann, K.: Benthic iron and phosphorus fluxes across the Peruvian oxygen  
942 minimum zone, *Limnol. Oceanogr.*, 57(3), 851–867, doi:10.4319/lo.2012.57.3.0851,  
943 2012.



- 944 Ohde, T.: Coastal Sulfur Plumes off Peru During El Niño, La Niña, and Neutral  
945 Phases, *Geophys. Res. Lett.*, 45(14), 7075–7083, doi:10.1029/2018GL077618, 2018.
- 946 Oschlies, A., Schulz, K. G., Riebesell, U. and Schmittner, A.: Simulated 21st  
947 century's increase in oceanic suboxia by CO<sub>2</sub>-enhanced biotic carbon export, *Global*  
948 *Biogeochem. Cycles*, 22(4), 1–10, doi:10.1029/2007GB003147, 2008.
- 949 Peng, Q., Xie, S.-P., Wang, D., Zheng, X.-T. and Zhang, H.: Coupled ocean-  
950 atmosphere dynamics of the 2017 extreme coastal El Niño, *Nat. Commun.*, 10(1),  
951 298, doi:10.1038/s41467-018-08258-8, 2019.
- 952 Pennington, J. T., Mahoney, K. L., Kuwahara, V. S., Kolber, D. D., Calienes, R. and  
953 Chavez, F. P.: Primary production in the eastern tropical Pacific: A review, *Prog.*  
954 *Oceanogr.*, 69(2–4), 285–317, doi:10.1016/j.pocean.2006.03.012, 2006.
- 955 Plummer, B. L. N., Parkhurst, D. L., Fleming, G. W. and Dunkle, S. A.: A computer  
956 program incorporating Pitzer's equations for calculation of geochemical reactions in  
957 brines., 1988.
- 958 Price, N. M. and Morel, F. M. M.: Cadmium and cobalt substitution for zinc in a  
959 marine diatom, *Nature*, 344(6267), 658–660, doi:10.1038/344658a0, 1990.
- 960 Ragueneau, O., Tréguer, P., Leynaert, A., Anderson, R. F., Brzezinski, M. A.,  
961 DeMaster, D. J., Dugdale, R. C., Dymond, J., Fischer, G., François, R., Heinze, C.,  
962 Maier-Reimer, E., Martin-Jézéquel, V., Nelson, D. M. and Quéguiner, B.: A review of  
963 the Si cycle in the modern ocean: Recent progress and missing gaps in the  
964 application of biogenic opal as a paleoproductivity proxy, *Glob. Planet. Change*,  
965 26(4), 317–365, doi:10.1016/S0921-8181(00)00052-7, 2000.
- 966 Raiswell, R. and Canfield, D. E.: The Iron Biogeochemical Cycle Past and Present,  
967 *Geochemical Perspect.*, 1(1), 1–220, doi:10.7185/geochempersp.1.1, 2012.
- 968 Rapp, I., Schlosser, C., Rusiecka, D., Gledhill, M. and Achterberg, E. P.: Automated  
969 preconcentration of Fe, Zn, Cu, Ni, Cd, Pb, Co, and Mn in seawater with analysis  
970 using high-resolution sector field inductively-coupled plasma mass spectrometry,  
971 *Anal. Chim. Acta*, 976, 1–13, doi:10.1016/j.aca.2017.05.008, 2017.
- 972 Rapp, I., Schlosser, C., Menzel Barraqueta, J.-L., Wenzel, B., Lüdke, J., Scholten, J.,  
973 Gasser, B., Reichert, P., Gledhill, M., Dengler, M. and Achterberg, E. P.: Controls on  
974 redox-sensitive trace metals in the Mauritanian oxygen minimum zone,



- 975 Biogeosciences Discuss., (November), 1–49, doi:10.5194/bg-2018-472, 2018.
- 976 Rickard, D., Griffith, A., Oldroyd, A., Butler, I. B., Lopez-Capel, E., Manning, D. A. C.  
977 and Apperley, D. C.: The composition of nanoparticulate mackinawite, tetragonal  
978 iron(II) monosulfide, *Chem. Geol.*, 235(3–4), 286–298,  
979 doi:10.1016/j.chemgeo.2006.07.004, 2006.
- 980 Rosenthal, Y., Lam, P., Boyle, E. A. and Thomson, J.: Precipitation and  
981 postdepositional mobility, *Earth Planet. Sci. Lett.*, 132, 99–111, doi:10.1016/0012-  
982 821X(95)00056-I, 1995.
- 983 Rue, E. L. and Bruland, K. W.: The role of organic complexation on ambient iron  
984 chemistry in the equatorial Pacific Ocean and the response of a mesoscale iron  
985 addition experiment, *Limnol. Oceanogr.*, 42(5), 901–910,  
986 doi:10.4319/lo.1997.42.5.0901, 1997.
- 987 Saito, M. A., Goepfert, T. J. and Ritt, J. T.: Some thoughts on the concept of  
988 colimitation: Three definitions and the importance of bioavailability, *Limnol.*  
989 *Oceanogr.*, 53(1), 276–290, doi:10.4319/lo.2008.53.1.0276, 2008.
- 990 Schlosser, C., Streu, P., Frank, M., Lavik, G., Croot, P. L., Dengler, M. and  
991 Achterberg, E. P.: H<sub>2</sub>S events in the Peruvian oxygen minimum zone facilitate  
992 enhanced dissolved Fe concentrations, *Sci. Rep.*, 8(1), 1–8, doi:10.1038/s41598-  
993 018-30580-w, 2018.
- 994 Schmidtko, S., Stramma, L. and Visbeck, M.: Decline in global oceanic oxygen  
995 content during the past five decades, *Nature*, 542(7641), 335–339,  
996 doi:10.1038/nature21399, 2017.
- 997 Scholz, F. and Neumann, T.: Trace element diagenesis in pyrite-rich sediments of the  
998 Achterwasser lagoon, SW Baltic Sea, *Mar. Chem.*, 107(4), 516–532,  
999 doi:10.1016/j.marchem.2007.08.005, 2007.
- 1000 Scholz, F., Severmann, S., McManus, J. and Hensen, C.: Beyond the Black Sea  
1001 paradigm: The sedimentary fingerprint of an open-marine iron shuttle, *Geochim.*  
1002 *Cosmochim. Acta*, 127, 368–380, doi:10.1016/j.gca.2013.11.041, 2014a.
- 1003 Scholz, F., Mcmanus, J., Mix, A. C., Hensen, C. and Schneider, R. R.: The impact of  
1004 ocean deoxygenation on iron release from continental margin sediments, *Nat.*  
1005 *Geosci.*, 7(6), 433–437, doi:10.1038/ngeo2162, 2014b.



- 1006 Scholz, F., Löscher, C. R., Fiskal, A., Sommer, S., Hensen, C., Lomnitz, U., Wuttig,  
1007 K., Göttlicher, J., Kossel, E., Steininger, R. and Canfield, D. E.: Nitrate-dependent  
1008 iron oxidation limits iron transport in anoxic ocean regions, *Earth Planet. Sci. Lett.*,  
1009 454, 272–281, doi:10.1016/j.epsl.2016.09.025, 2016.
- 1010 Schunck, H., Lavik, G., Desai, D. K., Großkopf, T., Kalvelage, T., Löscher, C. R.,  
1011 Paulmier, A., Contreras, S., Siegel, H., Holtappels, M., Rosenstiel, P., Schilhabel, M.  
1012 B., Graco, M., Schmitz, R. A., Kuypers, M. M. M. and LaRoche, J.: Giant Hydrogen  
1013 Sulfide Plume in the Oxygen Minimum Zone off Peru Supports  
1014 Chemolithoautotrophy, *PLoS One*, 8(8), doi:10.1371/journal.pone.0068661, 2013.
- 1015 Scor Working Group: GEOTRACES – An international study of the global marine  
1016 biogeochemical cycles of trace elements and their isotopes, *Geochemistry*, 67(2),  
1017 85–131, doi:10.1016/j.chemer.2007.02.001, 2007.
- 1018 Severmann, S., McManus, J., Berelson, W. M. and Hammond, D. E.: The continental  
1019 shelf benthic iron flux and its isotope composition, *Geochim. Cosmochim. Acta*,  
1020 74(14), 3984–4004, doi:10.1016/j.gca.2010.04.022, 2010.
- 1021 Sommer, S., Linke, P., Pfannkuche, O., Schleicher, T., Schneider v. D, D., Reitz, A.,  
1022 Haeckel, M., Flögel, S. and Hensen, C.: Seabed methane emissions and the habitat  
1023 of frenulate tubeworms on the Captain Arutyunov mud volcano (Gulf of Cadiz), *Mar.*  
1024 *Ecol. Prog. Ser.*, 382, 69–86, doi:10.3354/meps07956, 2009.
- 1025 Sommer, S., Gier, J., Treude, T., Lomnitz, U., Dengler, M., Cardich, J. and Dale, A.  
1026 W.: Depletion of oxygen, nitrate and nitrite in the Peruvian oxygen minimum zone  
1027 cause an imbalance of benthic nitrogen fluxes, *Deep. Res. Part I Oceanogr. Res.*  
1028 *Pap.*, 112(3), 113–122, doi:10.1016/j.dsr.2016.03.001, 2016.
- 1029 Stookey, L. L.: Ferrozine---a new spectrophotometric reagent for iron, *Anal. Chem.*,  
1030 42(7), 779–781, doi:10.1021/ac60289a016, 1970.
- 1031 Stramma, L., Johnson, G. C., Sprintall, J. and Mohrholz, V.: Expanding Oxygen-  
1032 Minimum Zones in the Tropical Oceans, *Science (80-. )*, 320(5876), 655–658,  
1033 doi:10.1126/science.1153847, 2008.
- 1034 Stramma, L., Schmidtko, S., Levin, L. A. and Johnson, G. C.: Ocean oxygen minima  
1035 expansions and their biological impacts, *Deep. Res. Part I Oceanogr. Res. Pap.*,  
1036 57(4), 587–595, doi:10.1016/j.dsr.2010.01.005, 2010.



- 1037 Straub, K. L., Benz, M., Schink, B. and Widdel, F.: Anaerobic, nitrate-dependent  
1038 microbial oxidation of ferrous iron. *Appl Environ Microbiol*, *Appl. Environ. Microbiol.*,  
1039 62(4), 1458–60, 1996.
- 1040 Sunda, W. G. and Huntsman, S. A.: Effect of Zn, Mn, and Fe on Cd accumulation in  
1041 phytoplankton: Implications for oceanic Cd cycling, *Limnol. Oceanogr.*, 45(7), 1501–  
1042 1516, doi:10.4319/lo.2000.45.7.1501, 2000.
- 1043 Sundby, B., Martinez, P. and Gobeil, C.: Comparative geochemistry of cadmium,  
1044 rhenium, uranium, and molybdenum in continental margin sediments, *Geochim.*  
1045 *Cosmochim. Acta*, 68(11), 2485–2493, doi:10.1016/j.gca.2003.08.011, 2004.
- 1046 Taylor, S. R. and McLennan, S. M.: Planetary crusts: Their composition, origin and  
1047 evolution , by Stuart Ross Taylor and Scott M. McLennan, *Meteorit. Planet. Sci.*,  
1048 44(3), 465–466, doi:10.1111/j.1945-5100.2009.tb00744.x, 2009.
- 1049 Thamdrup, B., Dalsgaard, T. and Revsbech, N. P.: Widespread functional anoxia in  
1050 the oxygen minimum zone of the Eastern South Pacific, *Deep Sea Res. Part I*  
1051 *Oceanogr. Res. Pap.*, 65, 36–45, doi:10.1016/j.dsr.2012.03.001, 2012.
- 1052 Turetta, C., Capodaglio, G., Cairns, W., Rabar, S. and Cescon, P.: Benthic fluxes of  
1053 trace metals in the lagoon of Venice, *Microchem. J.*, 79(1–2), 149–158,  
1054 doi:10.1016/j.microc.2004.06.003, 2005.
- 1055 Twining, B. S. and Baines, S. B.: The Trace Metal Composition of Marine  
1056 Phytoplankton, *Ann. Rev. Mar. Sci.*, 5(1), 191–215, doi:10.1146/annurev-marine-  
1057 121211-172322, 2013.
- 1058 Vedamati, J., Goepfert, T. and Moffett, J. W.: Iron speciation in the eastern tropical  
1059 south pacific oxygen minimum zone off peru, *Limnol. Oceanogr.*, 59(6), 1945–1957,  
1060 doi:10.4319/lo.2014.59.6.1945, 2014.
- 1061 Westerlund, S. F. G., Anderson, L. G., Hall, P. O. J., Iverfeldt, Å., Van Der Loeff, M.  
1062 M. R. and Sundby, B.: Benthic fluxes of cadmium, copper, nickel, zinc and lead in the  
1063 coastal environment, *Geochim. Cosmochim. Acta*, 50(6), 1289–1296,  
1064 doi:10.1016/0016-7037(86)90412-6, 1986.
- 1065 Xie, R. C., Rehkämper, M., Grasse, P., van de Fliedert, T., Frank, M. and Xue, Z.:  
1066 Isotopic evidence for complex biogeochemical cycling of Cd in the eastern tropical  
1067 South Pacific, *Earth Planet. Sci. Lett.*, 512, 134–146, doi:10.1016/j.epsl.2019.02.001,



- 1068 2019.
- 1069 Xu, Y., Feng, L., Jeffrey, P. D., Shi, Y. and Morel, F. M. M.: Structure and metal  
1070 exchange in the cadmium carbonic anhydrase of marine diatoms, *Nature*, 452(7183),  
1071 56–61, doi:10.1038/nature06636, 2008.
- 1072 Yücel, M., Sommer, S., Dale, A. W. and Pfannkuche, O.: Microbial sulfide filter along  
1073 a benthic redox gradient in the Eastern Gotland Basin, Baltic Sea, *Front. Microbiol.*,  
1074 8(FEB), 1–16, doi:10.3389/fmicb.2017.00169, 2017.
- 1075 Zago, C., Capodaglio, G., Ceradini, S., Ciceri, G., Abemoschi, L., Soggia, F.,  
1076 Cescon, P. and Scarponi, G.: Benthic fluxes of cadmium, lead, copper and nitrogen  
1077 species in the northern Adriatic Sea in front of the River Po outflow, Italy, *Sci. Total*  
1078 *Environ.*, 246(2–3), 121–137, doi:10.1016/S0048-9697(99)00421-0, 2000.
- 1079 Zumft, W. G.: Cell biology and molecular basis of denitrification., *Microbiol. Mol. Biol.*  
1080 *Rev.*, 61(4), 533–616 [online] Available from:  
1081 <http://www.ncbi.nlm.nih.gov/pubmed/9409151>  
1082 <http://www.pubmedcentral.nih.gov/articlerender.fcgi?artid=PMC232623>, 1997.
- 1083



1084 **Figure captions**

1085

1086 Fig. 1: Bathymetrical map of the Peruvian continental margin and sampling stations  
1087 along the latitudinal depth transect at 12° S. The sampling stations for pore water  
1088 profiles are depicted by white stars, for bottom water profiles by yellow dots and for  
1089 benthic chamber incubations by red dots.

1090 Fig. 2: Oxygen, nitrate, nitrite and hydrogen sulfide profiles on the Peruvian slope  
1091 (1000 m depth), crossing the oxygen minimum zone (upper panel), and the upper  
1092 shelf (75 m depth) (lower panel) during cruises M136 & M137 and M92 along the 12°  
1093 S transect.

1094 Fig. 3: Near bottom water profiles of dissolved Fe and Cd concentrations and  
1095 dissolved Fe to silicic acid ratios in the benthic boundary layer 0.5 m to 4 m above  
1096 the seafloor across the 12° S transect. Depicted by the red diamond is a second  
1097 sampling with a time difference of one month at station 1.

1098 Fig. 4: Pore water profiles of dissolved Fe(II) and hydrogen sulfide concentrations.  
1099 For station 7 (300 m water depth) and station 10 (950 m water depth) pore water  
1100 profiles are not shown to save space, but the diffusive fluxes are listed in table 2.  
1101 The profile of an earlier cruise, M92, at station 1 (75 m water depth) is displayed for  
1102 comparison. The uppermost sample of each profile represents the bottom water  
1103 concentration. All symbols are within error.

1104 Fig. 5: Dissolved Fe concentrations in incubated bottom waters from benthic chamber  
1105 incubations. The dashed line represents theoretical concentration gradients over the  
1106 incubation time based on our benthic diffusive fluxes (Table 2). All symbols are within  
1107 error.

1108 Fig. 6: Pore water profiles of dissolved Cd concentrations. The uppermost sample of  
1109 each profile represents the bottom water concentrations. All symbols are within error.

1110 Fig. 7: Dissolved Cd concentrations in incubated bottom waters from benthic  
1111 chamber incubations. The dashed line represents theoretical concentration gradients  
1112 over the incubation time based on our benthic diffusive fluxes (Table 3). All symbols  
1113 are within error.



1114 Fig. 8: Dissolved Fe, nitrate and nitrite concentrations in incubated bottom waters  
1115 from the benthic chamber incubation at station 4 (145 m water depth).

1116 Fig. 9: Comparison of benthic diffusive Fe(II) fluxes between cruises M136 & M137  
1117 and M92 on the Peruvian shelf. Negative values represent fluxes from the sediment  
1118 pore water into the bottom waters. Shaded bars on the upper panel display the  
1119 geochemical conditions in the water column during the time of sampling.

1120 Fig. 10: Schematic overview of how the mobility of different trace metal may respond  
1121 to an expansion of sulfidic conditions. Saturation indices (SI) were calculated for  
1122 different H<sub>2</sub>S concentrations and reported minimum and maximum concentrations of  
1123 trace metals in the water column (data from Bruland and Lohan 2003). Solubility  
1124 products for Fe (FeS ppt), Ni (Millerite), Zn (Wurtzite), Zn (Greenokite) were taken  
1125 from the Pitzer database (Plummer et al., 1988). The results are approximate since  
1126 concentrations instead of activities were used for calculations. A positive SI is  
1127 indicative of oversaturation whereas a negative SI is indicative of undersaturation.

1128

1129

1130

1131

1132

1133

1134

1135

1136

1137

1138

1139

1140

1141

Figure 2



1142 Table 1: Accuracy values for replicate concentration measurements ( $n = 7$ ) of certified  
1143 reference seawater for trace metals NASS-7 and CASS-6 by ICP-MS.

	NASS-7 certified value	NASS-7 measured value	CASS-6 certified value	CASS-6 measured value
Fe ( $\mu\text{g/L}$ )	$0.351 \pm 0.026$	$0.352 \pm 0.017$	$1.56 \pm 0.12$	$1.56 \pm 0.03$
Cd ( $\mu\text{g/L}$ )	$0.0161 \pm 0.0016$	$0.0162 \pm 0.0024$	$0.0217 \pm 0.0018$	$0.0216 \pm 0.0016$

1144

1145

1146

1147

1148

1149

1150

1151

1152

1153

1154

1155

1156

1157

1158

1159

1160



1161 Table 2: Comparison of benthic diffusive Fe(II) fluxes out of the sediment and  
 1162 geochemical bottom water conditions between M92 and M136 & M137 on the  
 1163 Peruvian shelf. Fluxes during M92 correspond to similar depth (see Fig. 9).

station	M136 & M137	M136 & M137	M136 & M137	M136 & M137	M136 & M137	M136 & M137	M92	M92
	water depth	latitude	longitude	bottom water condition	Fe(II) flux diffusive	Fe flux benthic chamber	bottom water condition	Fe(II) flux diffusive
	(m)	(S)	(W)		(mmol m <sup>-2</sup> y <sup>-1</sup> )	(mmol m <sup>-2</sup> y <sup>-1</sup> )		(mmol m <sup>-2</sup> y <sup>-1</sup> )
1	75	12°13.52	77°10.93	O <sub>2</sub> < 5 μM	-2.56	-1.74	slightly sulfidic	-22.69
3	130	12°16.68	77°14.95	nitrogenous	-0.81	-	slightly sulfidic	-3.16
4	145	12°18.71	77°17.80	nitrogenous	-17.08	-8.57	nitrogenous	-5.77
5	195	12°21.50	77°21.70	nitrogenous	-2.72	2.01	nitrogenous	-1.51
6	245	12°23.30	77°24.82	nitrogenous	-8.31	-5.43	nitrogenous	-10.20
7	300	-	-	nitrogenous	-3.02	-	nitrogenous	-3.12
9	750	12°31.35	77°35.01	O <sub>2</sub> > 5 μM	0.00	-6.11	O <sub>2</sub> > 5 μM	0.4
9	970	12°34.90	77°40.32	O <sub>2</sub> > 5 μM	-0.25	-1.68	O <sub>2</sub> > 5 μM	-0.12

1164  
 1165  
 1166  
 1167  
 1168  
 1169  
 1170  
 1171  
 1172  
 1173  
 1174



1175 Table 3: Comparison of sedimentary Cd excess compared to the lithogenic  
 1176 background and the contribution of Cd delivery to the sediment via different  
 1177 pathways: (1) diffusion across the sediment-water interface and Cd sulfide  
 1178 precipitation within the sediment; (2) Cd incorporation by phytoplankton and delivery  
 1179 to the sediment with organic matter; (3) Cd sulfide precipitation in the water column  
 1180 and particulate delivery to the sediment.

station	water depth (m)	Cd excess sediment <sup>1</sup> ( $\mu\text{mol m}^{-2} \text{y}^{-1}$ )	Cd flux diffusive ( $\mu\text{mol m}^{-2} \text{y}^{-1}$ )	Cd flux benthic chamber ( $\mu\text{mol m}^{-2} \text{y}^{-1}$ )	H <sub>2</sub> S surface in sediment below benthic chamber ( $\mu\text{M}$ )	Cd from organic matter <sup>2</sup> ( $\mu\text{mol m}^{-2} \text{y}^{-1}$ )	CdS precipitation in water column <sup>3</sup> ( $\mu\text{mol m}^{-2} \text{y}^{-1}$ )
1	75	248.87	-1.85	-1.6 (3109.5)*	641.02	8.34 - 49.04	199.83 - 240.53
3	130	153.41	0.83	-	-	4.87 - 17.40	135.19 - 147.72
4	145	35.07	0.52	13.4	1.30	1.55 - 6.48	28.07 - 32.99
5	195	44.76	0.72	22.6	9.52	5.71 - 7.71	36.36 - 38.36
6	245	35.15	0.55	21.2	0.40	3.60 - 6.54	28.06 - 31.00
9	750	4.44	-0.24?	0	0	1.48 - 3.21	1.23 - 2.96

1181

1182 <sup>1</sup> Calculated after Brumsack (2006) and multiplied with the mass accumulation rate  
 1183 for each site (Dale et al., 2015b).

1184 <sup>2</sup> Determined by multiplication of Cd to C ratio in average phytoplankton (Moore et al.,  
 1185 2013). For maximum values organic carbon rain rates and for minimum values  
 1186 organic carbon accumulation rates (Dale et al., 2015b) were used.

1187 <sup>3</sup> Remainder of Cd excess in sediment after subtraction of diffusive and organic Cd  
 1188 sources.

1189 \* Flux calculated from gradient of Cd bottom water concentration (0.5 m) and  
 1190 concentration in first benthic chamber incubation sample (0.25 h).

1191

1192



1193 Table 4: Modelled half-lives ( $t_{1/2}$ ) of dissolved Fe within the first 4 m distance from the  
1194 seafloor at station 3 (130 m water depth) and station 4 (145 m water depth) and data  
1195 used for determination of  $t_{1/2}$  using Eq. (4) and Eq. (5).

station	water depth	Si(OH) <sub>4</sub> flux benthic chamber ( $F_{Si}$ )	Si(OH) <sub>4</sub> concentration gradient ( $d_{Si}$ )	Eddy diffusion coefficient ( $K_y$ )	Modelled Fe at sediment surface ( $C_{BW}$ )	Fe oxidation constant ( $K_{Feox}$ )	Half-live in benthic boundary layer ( $t_{1/2}$ )
	(m)	( $\mu\text{mol cm}^{-2} \text{d}^{-1}$ )	( $\mu\text{mol cm}^{-3} \text{cm}^{-1}$ )	( $\text{m}^2 \text{s}^{-1}$ )	(nM)	( $\text{d}^{-1}$ )	(min)
3	130	0.73	$-4.05 \cdot 10^{-6}$	$1.5510^{-6}$	70	400	2.5
4	145	0.33	$-1.4410^{-6}$	$1.9610^{-6}$	81	3500	0.3

1196

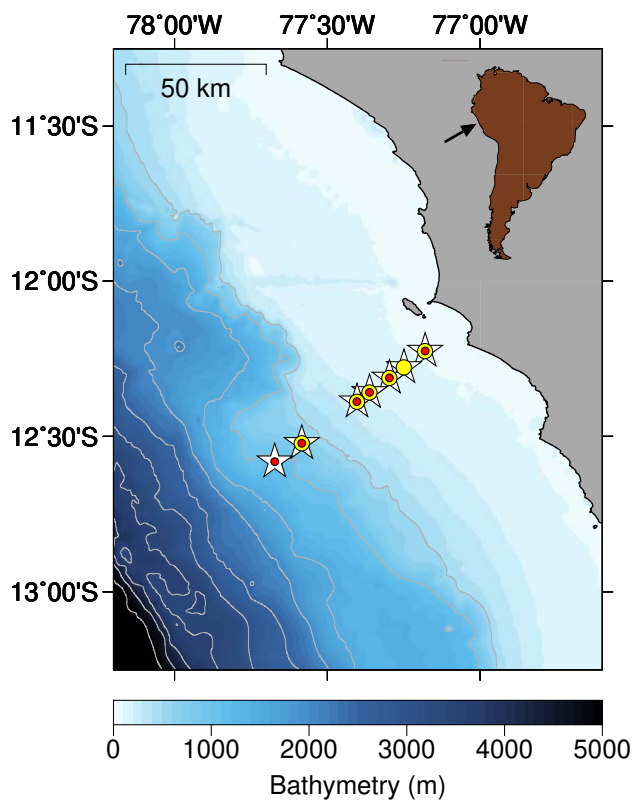


Figure 1

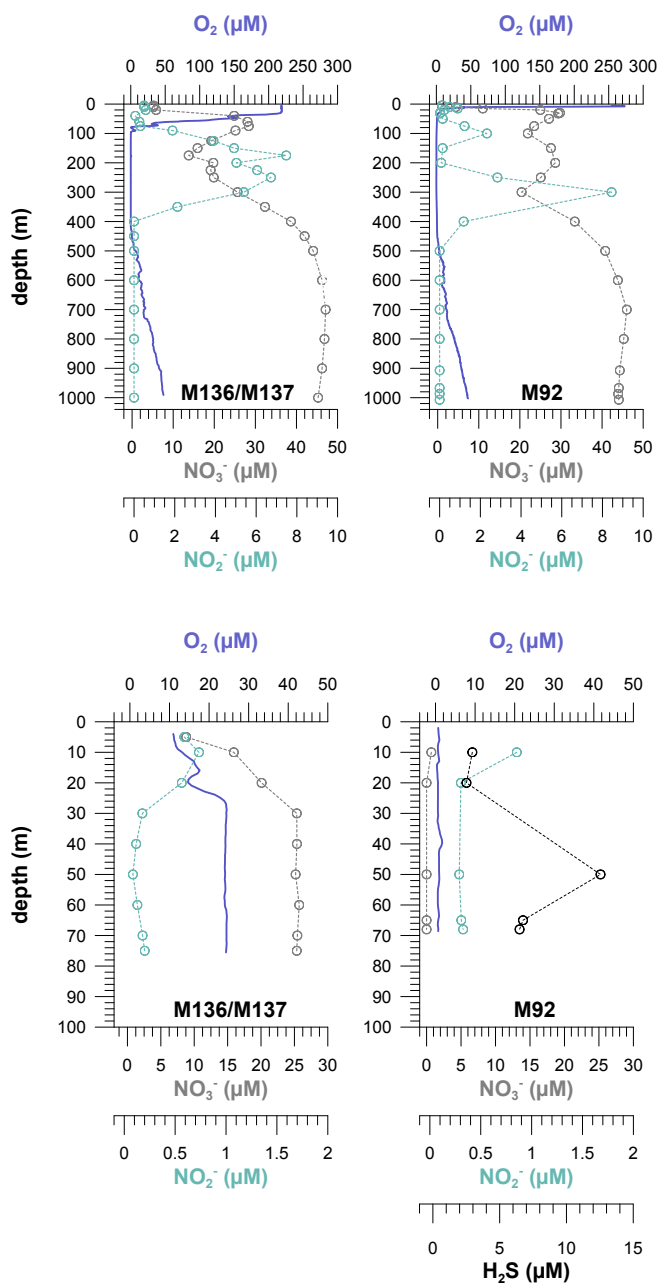


Figure 2

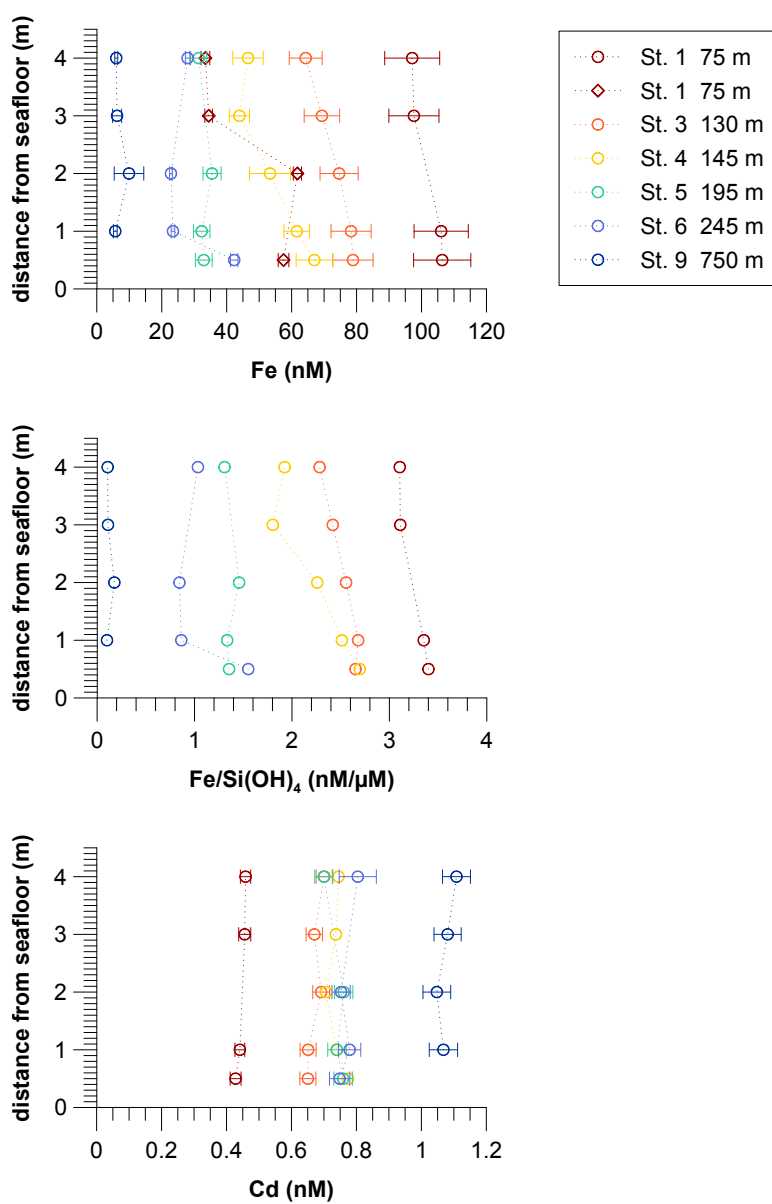


Figure 3

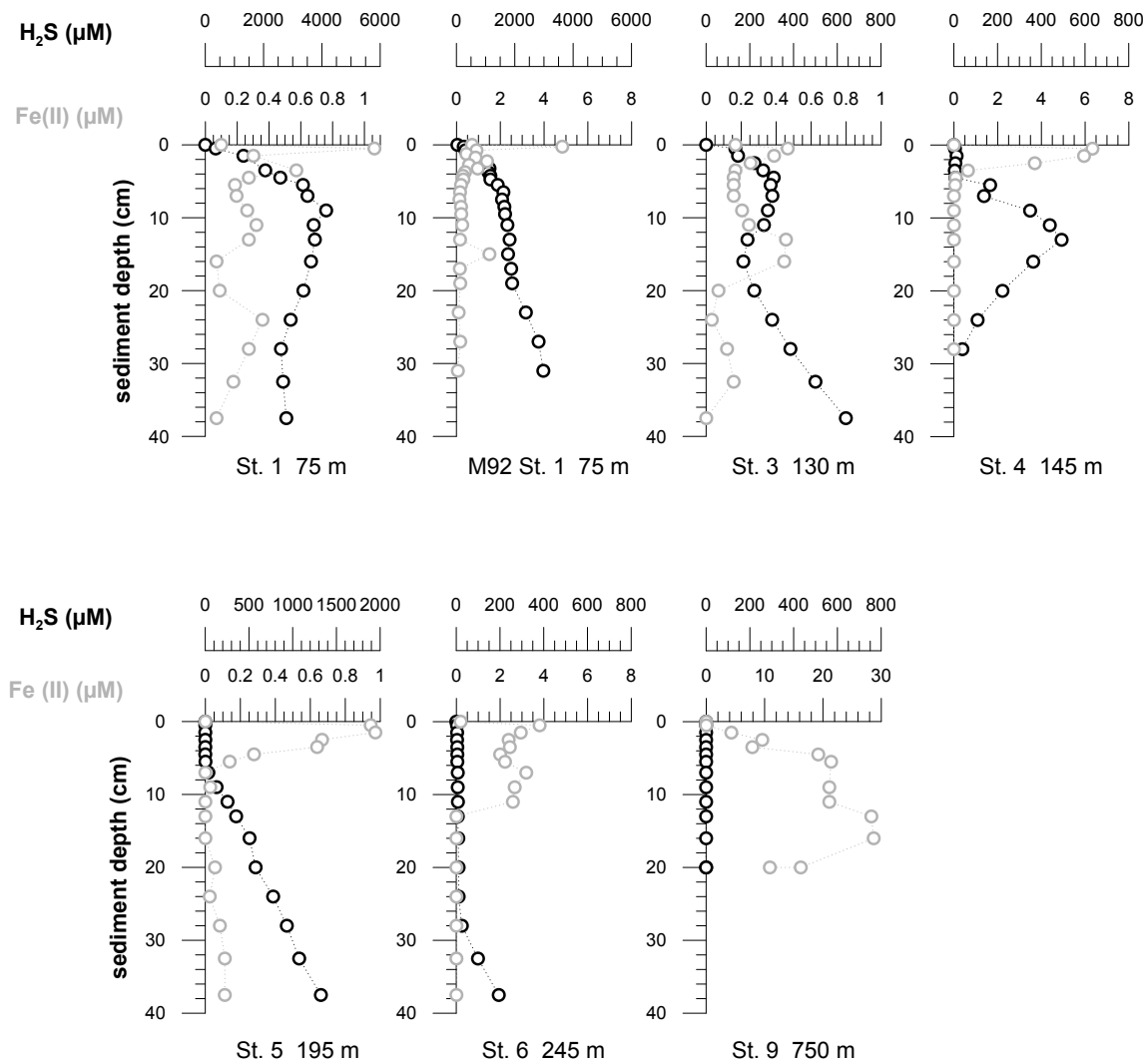


Figure 4

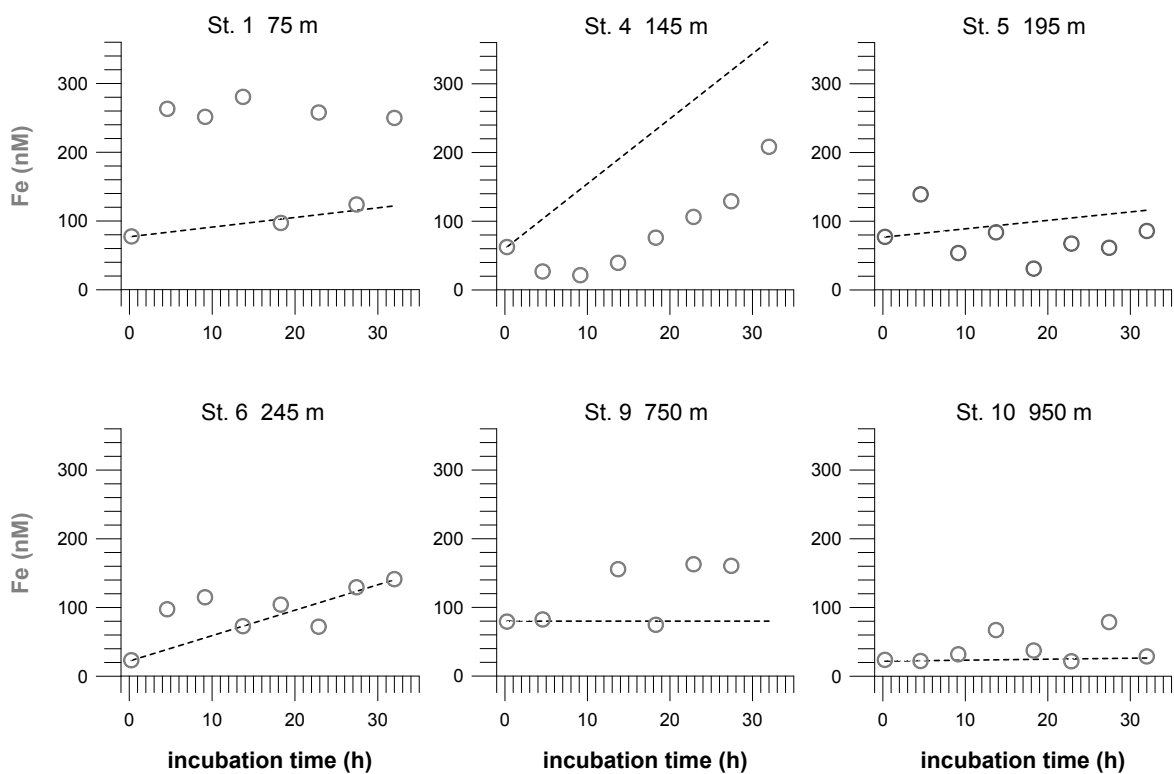


Figure 5

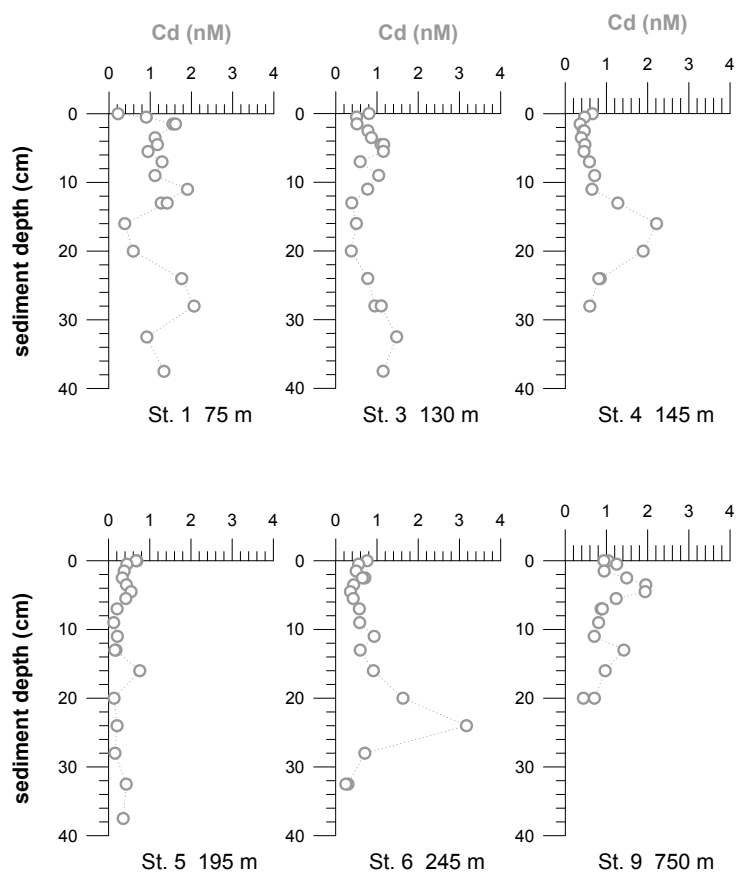


Figure 6

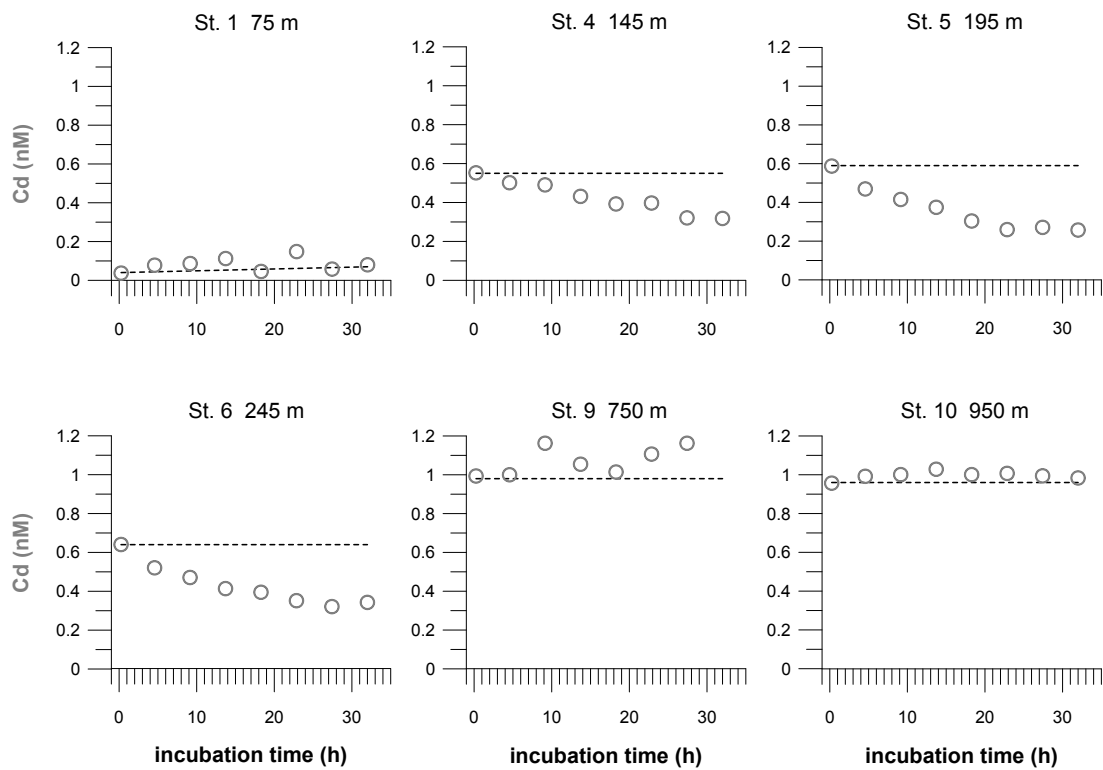


Figure 7

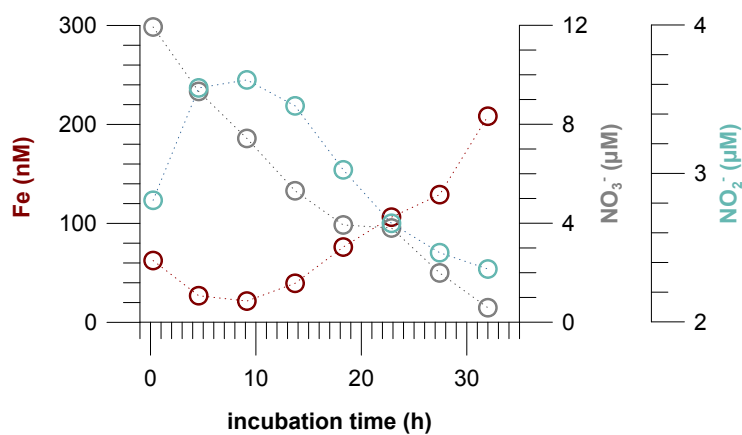


Figure 8

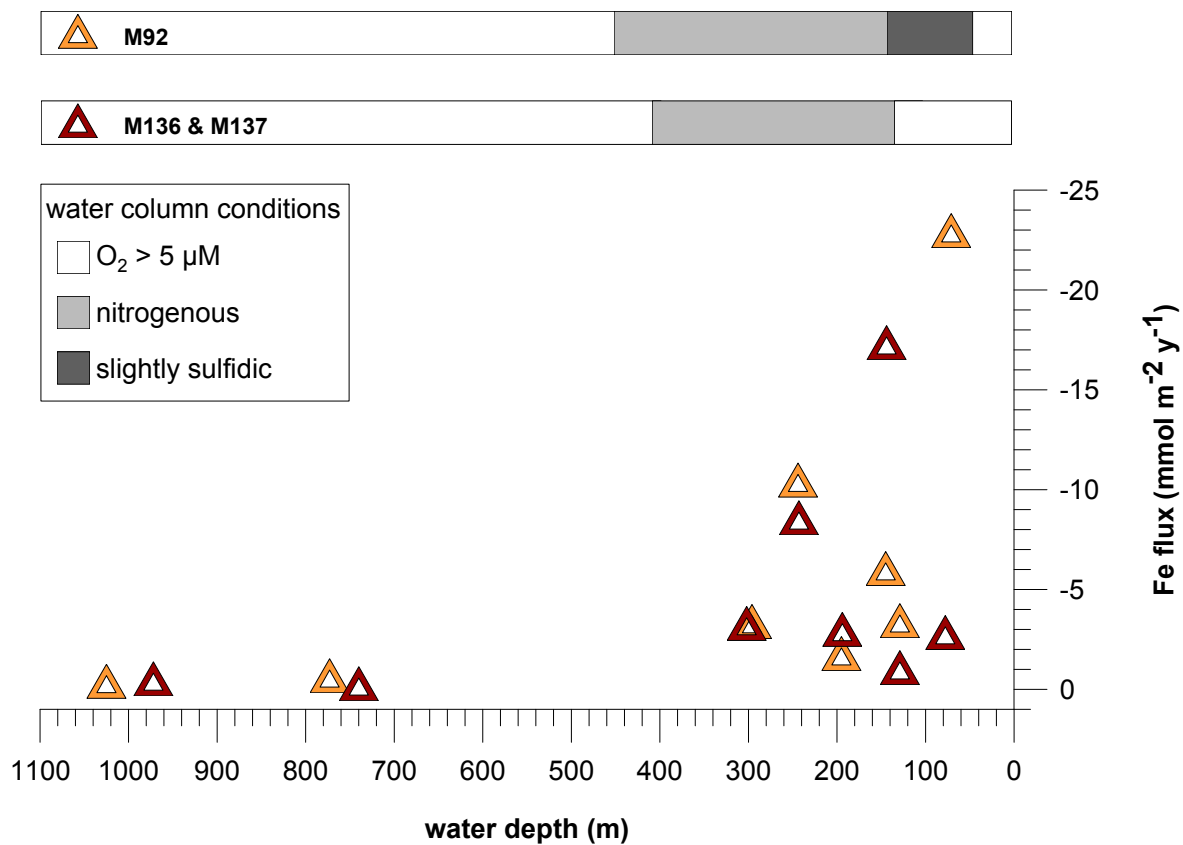


Figure 9

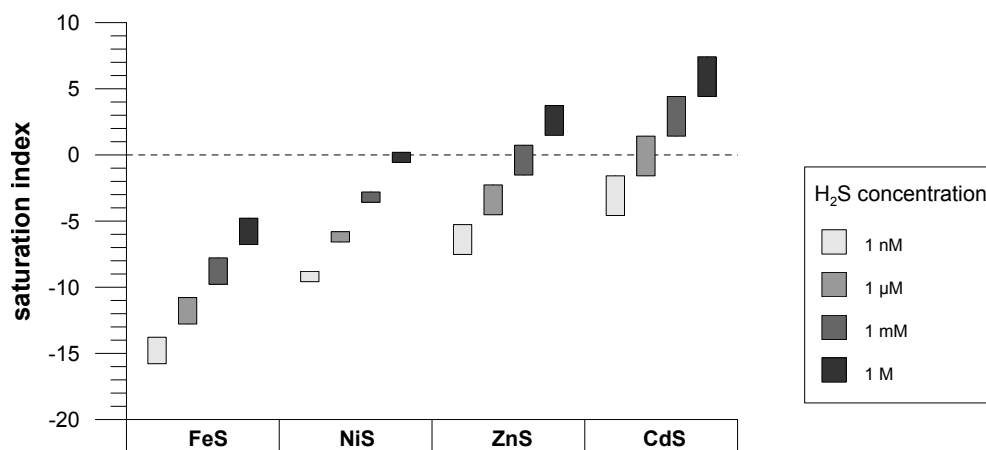


Figure 10